Atmos. Chem. Phys. Discuss., 14, 27881–27944, 2014
www.atmos-chem-phys-discuss.net/14/27881/2014/
doi:10.5194/acpd-14-27881-2014

Atmospheric Chemistry and Physics Discussions

Lidar profiling of aerosol optical properties from Paris to Lake Baikal (Siberia)

E. Dieudonné[1,*], P. Chazette[1], F. Marnas[1], J. Totems[1], and X. Shang[1]

[1]Laboratoire des Sciences du Climat et de l'Environnement (LSCE), CEA/CNRS/UVSQ, Gif-sur-Yvette, France
[*]now at: Laboratoire de Physico-Chimie de l'Atmosphère (LPCA), Université du Littoral, Côte d'Opale, Dunkerque, France

Received: 7 September 2014 – Accepted: 14 October 2014 – Published: 11 November 2014

Correspondence to: E. Dieudonné (elsa.dieudonne@univ-littoral.fr)

Published by Copernicus Publications on behalf of the European Geosciences Union.

Abstract

In June 2013, a ground-based mobile lidar performed the 10 000 km ride from Paris to Ulan-Ude, near Lake Baikal, profiling for the first time aerosol optical properties all the way from Western Europe to central Siberia. The instrument was equipped with N_2-Raman and depolarization channels that enabled an optical speciation of aerosols in the low and middle troposphere. The backscatter-to-extinction ratio (BER) and particle depolarization ratio (PDR) at 355 nm have been retrieved. The BER in the lower boundary layer (300–700 m) was found to be $0.017 \pm 0.009\,sr^{-1}$ in average during the campaign, with slightly higher values in background conditions near Lake Baikal ($0.021 \pm 0.010\,sr^{-1}$ in average) corresponding to dust-like particles. PDR values observed in Russian cities (> 1.7 %) are higher than the ones measured in European cities (< 1.3 %) due to the lifting of terrigenous aerosols by traffic on roads with a bad tarmac. Biomass burning layers from grassland or/and forest fires in southern Russia exhibit BER values ranging from 0.010 to $0.015\,sr^{-1}$ and from 2 to 3 % for the PDR. Desert dust aerosols originating from the Caspian and Aral seas regions were characterized for the first time, with a BER (PDR) of $0.022\,sr^{-1}$ (21 %) for pure dust, and $0.011\,sr^{-1}$ (15 %) for a mix between dust and biomass burning. The lidar observations also showed that this dust event extended over 2300 km and lasted for ~ 6 days. Measurements from the Moderate Resolution Imaging Spectrometer (MODIS) show that our results are comparable in terms of aerosol optical thickness (between 0.05 and 0.40 at 355 nm) with the mean aerosol load encountered throughout our route.

1 Introduction

Quantification of the aerosol radiative forcing still suffers from large uncertainties, making aerosols the dominant contribution in uncertainties on the anthropogenic influence on climate (IPCC, 2013). To improve the performances of climate models, observations are needed in order to provide better constraints from the regional to the global scale.

ACPD
14, 27881–27944, 2014

Large observational networks such as the Aerosol Robotic Network (AERONET; Holben et al., 1998), the Micropulse Lidar Network (MPLNET; Welton et al., 2001) or the Aerosol, Clouds and Trace gases Research Infrastructure Network (ACTRIS, formerly EARLINET; Matthias et al., 2004) provide the long-term measurement series needed to build a climatology of aerosol optical properties.

Complementarily, numerous large field experiments also took place over the past years to monitor long-range transport of aerosols and cover areas that do not host dense observation networks like oceans, South-East Asia, Africa or Arctic: for instance the Aerosol Characterization Experiments (ACE-1, ACE-2, ACE-Asia; Bates et al., 1998; Raes et al., 2000; Huebert et al., 2003), the Indian Ocean Experiment (INDOEX, Chazette, 2003), the African Monsoon Multidisciplinary Analysis (AMMA; Lebel et al., 2010), or the Polar study using Aircraft, Remote sensing, surface measurements and models, of Climate chemistry, Aerosols and Transport project (POLARCAT; Law et al., 2014). During those field campaigns, airborne measurements have been performed, which offer observations on a larger scale than ground-based stations.

On a smaller, regional scale, field experiments took place near large pollution hotspots like Mexico City, with the Megacity Initiative: Local And Global Research Observations project (MILAGRO, Molina et al., 2010), or Paris, with the Air Pollution Over the Paris Region project (ESQUIF, Vautard et al., 2003; Chazette et al., 2005), the Lidar pour la Surveillance de l'Air (LISAIR, Raut and Chazette, 2007) and the Megacities: emissions, urban, regional and Global Atmospheric Pollution and climate effects, and Integrated tools for assessment and mitigation project (MEGAPOLI, http://megapoli.dmi.dk/; Royer et al., 2011). Therefore, aerosol optical properties have been extensively documented over Western Europe and North America. On the other hand, Asia has drawn a growing attention as this region is becoming a larger contributor to aerosol anthropogenic emissions.

However, very few measurement programs exist over Russia, which for instance hosts only five stable AERONET stations while the country covers 11.5 % of the world's dry lands and contribute to aerosol emissions through large forest fires and several pol-

ACPD
14, 27881–27944, 2014

lution hotspots like Moscow (12 Mhab) or large industrial cities. Some measurement stations exist like the ZOTTO tower, located in the taiga 600 km North-West of Krasnoyarsk, where CO, particle concentration and aerosol optical properties are measured continuously up to 300 m a.g.l. since 2006 (Chi et al., 2013). Vertical profiles of particle concentration and extinction up to 5 km have been collected in the Tomsk region during an intensive flight campaign in 1986–1988, and then from monthly flights between 1999 and 2007 (Panchenko et al., 2012). At a larger scale, CO and particle concentrations have been measured during transcontinental flights in the framework of the Airborne Extensive Regional Observations in Siberia project (YAK-AEROSIB, Paris et al., 2010). However, most of the resulting observations took place in the free troposphere, and the flight plan was aimed towards the remote Northern Siberian regions rather than the industrial cities of Southern Siberia.

For other regions, and particularly for the industrial cities of Southern Siberia, only space-borne instruments offer a regular coverage, for instance the Moderate Resolution Imaging Spectrometer (MODIS, e.g. King et al., 1992; Salomonson et al., 1989) or the Polarization and Directionality of the Earth Reflectance/Polarization and Anisotropy of Reflectances for Atmospheric Sciences coupled with Observations from a Lidar (POLDER/PARASOL, e.g. Deuzé et al., 2001) or the Cloud-Aerosol Lidar and Infrared Pathfinder Satellite Observation (CALIPSO, e.g. Chazette et al., 2010; Winker et al., 2003). However, observations are limited by cloud coverage and by the satellite overpass time, so that ground-based observations are welcome to better document aerosols over Russia.

In June 2013, we performed the first road transect through Europe and Russia for aerosol profiling, with a Raman lidar instrument embedded on a van going all the way from Paris to Lake Baikal. This campaign offers a unique snapshot of aerosol optical properties from Western Europe to Eastern Russia, which can be extrapolated in a broader climatological vision through satellite observations. This article is the first one of the pair that will describe the results obtained during this campaign; it has two main objectives. Firstly, it aims at presenting the general variability of the aerosol nature,

ACPD
14, 27881–27944, 2014

amount and optical properties along the journey. For this purpose, a systematic data treatment is used whose precision is limited by the need to apply it both to the nighttime and to the daytime, noisier data. For this reason, in a second time, a finer characterization of the optical properties of the desert dust and biomass burning aerosols encountered in Russia will be presented, based on a few case studies using best quality data.

Therefore, this paper is organized as follow. Section 2 presents the itinerary of the campaign, the lidar instrument and the data processing methods used to retrieve the aerosol extinction, Backscatter to Extinction Ratio (BER) and Particle Depolarization Ratio (PDR). Then, Sect. 3 presents the variability of aerosols along the journey, the particle nature being identified through the combination of the two intensives properties that are the BER and PDR. Section 3 also analyzes the representativeness of the observations in regards to longer time series of space-borne measurements. Finally, Sect. 4 presents a few case studies on which it was possible to perform a finer characterization of the optical properties (BER and PDR) of the dust and biomass burning particles encountered during the route, and the origin of those particles is also discussed. The finer characterization of the anthropogenic particles encountered over the various pollution hot-spots along the journey will be presented in the up-coming second paper.

2 Experimental setup and method

2.1 Itinerary and instrumentation

The van carrying the lidar instrument departed from Paris on 4 June 2013 and reached Lake Baikal on 28 June. Afterwards, fixed location measurements were performed on the lake shore, in Istomino village (52.128° N, 106.287° E), and mobile observations were recorded during round trips between Istomino and Ulan-Ude city, 80 km South-East of the Lake. Ground-based mobile measurements, though limited by bat-

ACPD
14, 27881–27944, 2014

tery power, could be conducted during most of the journey (during daytime). Fixed location measurements took place during most of the stop-overs (during nighttime) using local power supply so that rain showers and low-level clouds were the main limiting factors.

An overview of the van itinerary and of the lidar data availability can be found on Fig. 1, over a map of PM_{10} emissions extracted from the Emission Database for Global Atmospheric Research (EDGAR v4.2, http://edgar.jrc.ec.europa.eu/). The journey went through a number of pollution hotspots: Paris, the Rhine Valley, Berlin, Warsaw, Moscow, and several large and industrial Russian cities such as Nizhniy-Novgorod, Kazan, Ufa, Chelyabinsk, Omsk, Novosibirsk, Krasnoyarsk and Irkutsk. Regarding wildfires, three main vegetation types susceptible to produce biomass burning aerosols were encountered: first, temperate forest dominate in the Baltic countries and western Russia, then the vegetation turns into grasslands in the steppes of southern Russia (from Nizhniy-Novgorod to Omsk, except in the Ural Mountains) and finally boreal forest occupies all the eastern part of the journey (and also the Ural Mountains between Ufa and Chelyabinsk).

The lidar instrument used during the campaign is similar to the one previously described by Royer et al. (2011). It operates at 355 nm with 15 mJ emitted energy by pulse, and has three acquisition channels for elastic, depolarization and N_2-Raman backscatters. The signals were recorded with an initial resolution of 25 s (500 laser shots) and 0.75 m, before being averaged over 5 or 30 min and 7.5 m in altitude. A systematic treatment was performed on the 30 min average profiles from the whole campaign to analyze the variability of the Backscatter to Extinction Ratio (BER) in the lower troposphere (Sect. 2.2.3). For dust or biomass burning events, a more complete processing is performed to retrieve the full BER profile (Sect. 2.2.2 and 2.2.4). The retrieval of the particle depolarization ratio (PDR) is described in Sect. 2.3.

ACPD
14, 27881–27944, 2014

2.2 Retrieval of the aerosol extinction and Backscatter to Extinction Ratio (BER)

2.2.1 Lidar equations

After correction for the sky background, the solid angle and the overlap function, the range-corrected signals S_i measured at wavelength λ_i ($i = \mathrm{e}, \mathrm{r}$ for the elastic and N_2-Raman channels respectively) and at the altitude z for a vertically pointing lidar can be written under the form (Measures, 1984):

$$S_\mathrm{e}(z) = K_\mathrm{e} \cdot [\beta_\mathrm{p}(\lambda_\mathrm{e}, z) + \beta_\mathrm{m}(\lambda_\mathrm{e}, z)] \cdot \exp\left(-2\int_0^z [\alpha_\mathrm{p}(\lambda_\mathrm{e}, s) + \alpha_\mathrm{m}(\lambda_\mathrm{e}\, s)]\mathrm{d}s\right) \quad (1)$$

$$S_\mathrm{r}(z) = K_\mathrm{r} \cdot \beta_{\mathrm{N}_2}(\lambda_\mathrm{r}, z) \cdot \exp\left(-\int_0^z [(1+\eta)\alpha_\mathrm{p}(\lambda_\mathrm{e}, s) + \alpha_\mathrm{m}(\lambda_\mathrm{e}, s) + \alpha_\mathrm{m}(\lambda_\mathrm{r}, s)]\mathrm{d}s\right) \quad (2)$$

with $\eta = (\lambda_\mathrm{r}/\lambda_\mathrm{e})^{-a}$.

The K_i are the instrumental constants which include contributions of optical reflections/transmissions, quantum efficiency of the detectors, amplification gains, laser energy and reception area. β and α are the backscatter and extinction coefficients, the subscripts p or m standing for the particular and molecular contributions respectively. β_{N_2} is the Raman backscatter coefficient, which is proportional to the air density ρ (the Raman backscatter differential cross-section and N_2 mixing ratio being constant with altitude in the troposphere). Aerosol extinction coefficients at the emitted and Raman wavelength are linked by the Ångström exponent a (Ångström, 1964); a constant value of $a = 1$ was used over the journey. Indeed, only sun-photometers can provide Ångström values in the UV wavelengths (MODIS only provides the coefficient between its 470 and 660 nm channels) and the van journey came close to only four AERONET stations over the 10 000 km. In the absence of experimental data, using an average value of 1 appears as a good compromise (as the residual relative uncertainty was

ACPD
14, 27881–27944, 2014

calculated to be less than 3 %; Chazette et al., 2014). The molecular extinction and backscatter coefficients are determined using a reference atmospheric density profile and a polynomial interpolation between the 40 levels of the profile (Royer et al., 2011 and references therein). The effects of the molecular extinction α_m are corrected in the signals S_i to give S'_i.

The particle extinction α_p and backscatter β_p coefficients are the two unknowns of the lidar equation. Using the Raman signal, which depends only on the extinction, it is possible to retrieve separately both coefficients and determine the Backscatter to Extinction Ratio $k_p = \beta_p/\alpha_p$. The BER is the inverse of the more commonly used Lidar Ratio (LR); it was preferred as it is more directly linked to the single scattering albedo of aerosols, which is one of the most important parameter to determine their radiative impact on climate. The BER (or LR) is an intensive property that does not depend on the particle concentration but is linked to their microphysical and chemical characteristics; it is therefore very useful to identify the aerosol nature.

To retrieve the particle extinction coefficient from the Raman signal, the intermediate function $Q_r(z)$ is used:

$$Q_r(z) = -\frac{1}{1+\eta} \ln\left[\frac{S'_r(z)}{\rho(z)}\right] = \tau_p(0,z) - K'_r \quad (3)$$

where τ_p is the cumulative particle extinction, i.e. the aerosol optical thickness (AOT) between the ground and altitude z. Constant K'_r includes the instrumental constant K_r, the N_2 mixing ratio, the Raman backscatter differential cross-section and coefficient η (e.g. Chazette et al., 2014). More generally, the AOT between two altitudes z_1 and z_2 is defined and related to Q_r following:

$$\tau_p(z_1,z_2) = \int_{z_1}^{z_2} \alpha_p(s)\,ds = Q_r(z_2) - Q_r(z_1) \quad (4)$$

ACPD
14, 27881–27944, 2014

The wavelength dependency of α_p and τ_p is now omitted as S'_r does not depend on λ_r anymore. Note that the way K'_r is dealt with depends if the Raman signal is exploitable up to a purely molecular layer or not: if the Signal to Noise Ratio (SNR) is too low, only the lower part of the profile will be used.

2.2.2 Raman inversion for case studies

When using nighttime data and long averaging periods, the Raman channel can range easily up to 5 km and reach a purely molecular layer. In this case, constants K_e and K'_r are removed by normalizing the signals at the altitude z_0 of the molecular layer, so that the profile of aerosol backscatter coefficient is computed directly following:

$$\beta_p(z) = \beta_m(z_0) \cdot \frac{S'_e(z)}{S'_e(z_0)} \cdot \exp\left(-Q_r(z) + Q_r(z_0)\right) - \beta_m(z) \quad (5)$$

Theoretically, the extinction coefficient could be retrieved simply by differentiating the optical depth profile ($\alpha_p = \mathrm{d}\tau_p/\mathrm{d}z$) as in Ansmann et al. (1990). However, differentiating noisy signals is not possible as it dramatically increases the resulting noise level. One possible solution is to use a low-pass derivative filter like a Savitzky–Golay filter (Savitzky and Golay, 1964, applied for instance in Pappalardo et al., 2004) or a Kaiser filter (Kaiser and Reed, 1977, applied for instance by Ferrare et al., 1998). Another possible solution is to use first or second order polynomial curve fitting on a sliding window (e.g. Pappalardo et al., 2004; Whiteman, 1999). Note that slope estimation using local polynomial fits can be reduced to a digital filter, making these solutions somewhat equivalent. Finally, the BER profile can be retrieved using a regularization method such as the one proposed by Tikhonov and Arsenin (1977), as was applied for instance by Royer et al. (2011). Low-pass derivative filters and sliding polynomial fits are the most commonly and longest used methods. Besides being easier to implement, their advantage is that the extinction coefficient and BER values retrieved at different altitudes are independent, though the effective vertical resolution is always degraded by this pro-

ACPD
14, 27881–27944, 2014

cess. Regularization methods are more complicated to implement especially because it is difficult to automatize the choice of the regularization parameter. Moreover, the disadvantage of these methods is that the regularized profile is a global solution, implying that an outlier can perturb the extinction coefficient and BER values at all altitudes.

Here, we use a low-pass derivative filter which kernel is based on the first derivative of a Gaussian curve (ter Haar Romeny et al., 1993). The magnitude of the transfer function of such a filter is presented on Fig. 2 for a filter width σ of 4 points (30 m). The transfer functions of a 4th order Savitzky–Golay filter and of a linear least-square fit filter are also presented. To make the comparison easier, the kernel size of both filters has been adjusted to obtain the same cut-off frequency as the Gaussian filter ($\sim 11\,\mathrm{km}^{-1}$), the cut-off frequency being defined as the frequency at which the filter response reaches $1/e$ of its maximum amplitude. Figure 2 clearly shows that the rejection of high frequencies, i.e. short-scale fluctuations in the extinction, is much better with the Gaussian filter than with the Savitzky–Golay or linear fit filter (the difference is around 30 dB after $20\,\mathrm{km}^{-1}$).

To take into account the decrease of the SNR with increasing altitude, the filter width σ is increased following a saturating exponential function $\sigma(z) = a + b \cdot \left(1 - \exp(-z/1.5)\right)$ with z the altitude a.g.l. in km. Usually, the pair $a = 3$ and $b = 7$ produces good results, but if the aerosol load is low or if the averaging time is short, b can be increased up to 19 or 24 (in which case, a is reduced to 1 so as to avoid too large σ values in the lowest layers). The effective vertical resolution of the resulting extinction profile is presented on Fig. 3 for the three sets of parameters (the effective resolution is defined as the inverse of the cut-off spatial frequency). With $a = 3$ and $b = 7$, the vertical resolution tends towards 200 m at 5 km a.g.l., while the pair $a = 1$ and $b = 24$ will be used to produce a coarse resolution profile (~ 500 m) in low SNR conditions.

ACPD
14, 27881–27944, 2014

2.2.3 Single layer constrained Klett inversion for systematic treatment

During daytime, the range of the N_2-Raman channel is greatly limited by the sky background. With a 30 min averaging period, the signal is exploitable up to 700 m a.g.l. in the worst conditions, i.e. around noon. Using longer time averages enables only a limited improvement (900 m a.g.l. for 1 h averages) and leads to mix data recorded over long distances, i.e. in potentially heterogeneous atmospheric conditions. The speed limits being 90 km h^{-1} (110 km h^{-1} on western motorways), in 30 min, the van travels by a maximum of 45 km (55 km in Western Europe), which is a good compromise for spatial averaging. Data from the whole campaign produced 560 distinct 30 min average cloudless profiles that were all processed as described below.

First, the Raman channel is used to determine the partial AOT between 300 m (complete overlap) and 700 m a.g.l. (range limit). The partial AOT is not computed directly using Eq. (4) as such a derivative is rather sensitive to noise, even after smoothing Q_r and using an average over several points around z_1 and z_2. Instead, a linear fit of Q_r is performed over the 300–700 m a.g.l. range, which slope is the average extinction coefficient in the aerosol layer. Then, multiplying this result by the layer depth gives the partial AOT.

In a second step, the partial AOT is used to constrain the BER used in the Klett inversion (Klett, 1985). The principle is the same as described in Royer et al. (2011), except that the convergence is not dealt with using a dichotomy algorithm. Indeed, the partial AOT in the lowest layers also depends on the transmission by the upper layers so that the partial AOT is not always a monotonic function of the BER, especially when elevated layers of aerosols are present. Instead, the extinction profile is inverted using 20 BER values distributed from 0.005 to 0.1 sr^{-1} (i.e. LR: lidar ratios – extinction-to-backscatter ratios – from 10 to 200 sr) as this range covers BER values observed in the literature for the main types of aerosols (Tables 1–3). Then, the interval is narrowed between the two BER values that produce the partial AOT values closest to the Raman constraint and the process is repeated.

ACPD
14, 27881–27944, 2014

After three iterations, the BER value giving the best agreement between the constraint and the inverted partial AOT is chosen; then, the BER is known by 10^{-4} sr^{-1} and the agreement is better than 10^{-3}, if a solution exists. Indeed, there is not always a BER value which allows to reproduce the Raman partial AOT, either because the constraint layer is not homogeneous, or because elevated layers are present and contain aerosols of a different type than in the PBL (with a very different BER value). In this case, reaching convergence in the lowest layers would require a manual set-up of the BER in the upper layers, which is not compatible with an automatic data processing.

According to the sensitivity study carried out by Royer et al. (2011), the main source of uncertainty on the BER value is the random detection processes. It leads to a relative error on the BER ranging between 4 and 18 % (16 to 100 %) during nighttime (daytime) for AOT values ranging from 0.1 to 0.5 and with a SNR of 35 (10). For the lidar-derived AOT the relative uncertainty stands between 4 and 16 % (12 to 40 %) during nighttime (daytime) for the same SNR. In this paper, the uncertainty is assessed using a Monte-Carlo process: the photon noise at detection is propagated throughout the inversion process to give an estimation of the resulting error on the extinction coefficient profile and BER value (or profile).

2.2.4 Multi-layer constrained Klett inversion

When the Raman channel has a longer detection range than 700 m a.g.l. (during nighttime), the process described in the previous section can be applied over several successive layers. At first, the constraint zone is located just below the normalization zone, or just below the limit range of the Raman channel. The BER value giving the best agreement between the partial AOT from the Raman channel and from Klett's inversion is determined and attributed to this layer. Then, the constraint zone is translated downwards and the process is repeated until reaching the ground level. Layers where the aerosol load is too small (average extinction coefficient lower than 0.02 km^{-1}) are ignored and the BER from the layer located directly above them is kept. The constraint zone width depends on the aerosol load and varies from 200 to 900 m; the altitude

ACPD
14, 27881–27944, 2014

shift from one step to the next is between 1 and 1/3 of the constraint zone width. The case studies that will be presented in Sect. 4 show that this method gives similar results as the derivative Raman inversion, with the advantage of producing a smoother BER profile (no fluctuations in the layers with low aerosol load). Therefore, the case study process is constructed as follows: first, we determine BER profiles from a long time average profile (at least 1 h) using both methods and then, we use the BER profile from the sliding-window converging process to inverse the 5 min average profiles and retrieve the extinction coefficient.

2.3 Retrieval of the Particle Depolarization Ratio (PDR)

The volumetric depolarization ratio (VDR) was determined following the procedure described in Chazette et al. (2012) i.e. using the plate transmission and reflection coefficients measured in the lab before departure, along with the gain ratio between the total and perpendicular polarization channels. The gain ratio value was calibrated using measurements obtained next to Lake Baikal during one night when the atmosphere was devoid of any elevated aerosol layer. Several tests that have been carried on other days earlier during the campaign showed that the gain ratio was stable over time, so that the value obtained from the Lake Baikal experiment was used during the whole campaign. The particle depolarization ratio (PDR) is then computed as in Chazette et al. (2012) with a relative uncertainty that increases from 9 to 24 % with AOT values decreasing from 0.34 to 0.08. As the PDR is a physical parameter without meaning when there are no aerosols, its calculation is performed only for layers where the scattering ratio (defined as the ratio of the total to molecular backscatter coefficients) is at least 1.005.

ACPD
14, 27881–27944, 2014

3 Variability of aerosols along the transect

In order to analyze the aerosol variability along the transect, data from the whole campaign are processed using a systematic treatment whose details are summarized in Sect. 3.1. The next section (Sect. 3.2) aims at highlighting the general features of the campaign and identifying the case studies by studying the spatial distribution of aerosols along the transect. The latter is analyzed in terms of amount (optical thickness) and depolarization, which is a first sorting criterion between terrigenous and carbonaceous particles. A finer classification of the particle types encountered during the campaign is proposed in Sect. 3.3, based on the Backscatter to Extinction Ratios (BER) and Particle Depolarization Ratios (PDR) retrieved in the boundary layer using the systematic data treatment. Finally, the representativeness of the campaign period is assessed by comparison with longer time series of space-borne observations and ground sunphotometers (Sect. 3.4).

3.1 Retrieval process for the systematic analysis

As explained in Sect. 2.2.3, the systematic analysis of data recorded during the whole campaign relies on 30 min average profiles, which leads the N_2-Raman channel to be exploitable up to 700 m from the lidar in all conditions. The partial optical thickness derived from the N_2-Raman channel is used to constrain the BER in the 300–700 m layer following the convergent Klett procedure described in Sect. 2.2.3. However, convergence is reached for only 193 (34.5 %) of the 560 30 min average profiles. As explained in Sect. 2.2.3, this is not surprising because the constraint only bears on the lower PBL, so that the process does not work in a heterogeneous atmosphere. This is for instance the case if the humidity in the upper PBL is higher than at ground level and contributes to aerosols growth, or if an elevated layer containing another type of aerosol is present.

When a BER value fitting the constraint provided by the N_2-Raman channel cannot be retrieved, it is necessary to choose an arbitrary BER value in order to compute the

ACPD
14, 27881–27944, 2014

aerosol optical thickness (AOT) that will be used to study the variability of aerosols along the transect. In order not to introduce discontinuities in the AOT dataset between profiles that converged or not, the same BER value is used to invert all profiles through a standard Klett procedure. The chosen BER is the average obtained over the 193 converging profiles ($0.017 \pm 0.009\,sr^{-1}$), a value that will be discussed in Sect. 3.3, along with the distribution of BER values.

As the computation of the Particle Depolarization Ratio (PDR) depends on the inverted profile of aerosol backscatter, this also raises the question of choosing an arbitrary BER value to treat the profiles that did not converge. Therefore, and again to avoid discontinuities in the PDR dataset, the depolarization is also determined using the campaign average BER. The uncertainty associated with this hypothesis can be assessed only when and where the Raman channel provided a constrained BER that could be used to compute a reference PDR value. This reduces the ensemble to the 193 converging profiles, and to the 300–700 m layer used to constrain the BER. The detailed discussion about the uncertainties is presented in Sect. 3.3, along with the BER and PDR distributions. As it appears that 90 % of the PDR values are affected by a variation of less than 0.9 % when the constrained BER value is replaced by the campaign average BER, we believe that this latter value can be used to discuss the general distribution of PDR values along the transect.

3.2 Identification of general features on the spatial distribution of aerosols

In order to discuss the horizontal distribution of aerosols along the transect, Fig. 4 presents the map of AOT values obtained when inverting all the 30 min average profiles using the campaign average BER value of $0.017 \pm 0.009\,sr^{-1}$ (see Sect. 3.1). Profiles recorded within a radius of 15 km are grouped and replaced by their average profile, which leaves 123 profiles. The method chosen to discuss the vertical distribution of aerosols and their nature was to compute the partial AOT and the average PDR below and above a fixed level. An altitude of 1500 m a.g.l. was chosen as it can be considered as an average value for continental PBL or residual layer top, i.e. the maximum altitude

ACPD
14, 27881–27944, 2014

influenced by the ground. The partial AOT and the average PDR values as a function of longitude are presented on Fig. 5. Values of PDR above 1500 m a.g.l. are scarce because this ratio cannot be computed for profiles gathered around noon (the depolarization channel SNR is too low) or when the aerosol load is too small in the free troposphere. Combustion aerosols from pollution or biomass burning are found with PDR values below 5 % at 355 nm while aerosol mix dominated by dust-like particles usually have PDR values above 10 % (Burton et al., 2012; Müller et al., 2007). Median values cannot be attributed certainly to the previous types of aerosols and indicate most probably a mixture of these particles.

In Europe (longitude < 26° E), PDR values in big cities such as Paris and Berlin are below 1 %, indicating the preponderance of pollution aerosols, while PDR values in the rural regions of Central Germany are slightly higher (< 2.1 %). Over Germany and Poland (particularly near Frankfurt, Berlin and Warsaw), higher values of free tropospheric AOT show the presence of elevated aerosols layers with PDR values similar to those found in the PBL, suggesting that this is probably pollution lifted up and transported from another part of Europe. In Russian cities, the urban PBL is generally characterized by higher PDR values (2–4 %) as compared to European cities (PDR < 1 % in Paris PBL), which indicates that the particle composition results from a mixture of traffic and industrial emissions with terrigenous aerosols. Indeed, Russian cities East of Moscow appear much dustier than European cities due to bad road tarmac and lack of vegetation on traffic islands, which results in a lot of terrigenous aerosols being lifted up by road traffic and injected in the urban PBL.

Between Kazan and Ufa (47–57° E), an obvious desert dust event is visible, associated with PDR values reaching 37 % above 1500 m and 18 % below, where the dust layer was observed to mix into the PBL. The highest AOT values (up to 0.43, associated with up to 70 % of the AOT above 1500 m a.g.l.) were observed farther East, between Ishim and Omsk. However, the PDR values (5–9 %) indicate that a mixing has occurred with combustion aerosols, most probably of biomass burning origin since the region is

ACPD
14, 27881–27944, 2014

very isolated. Above Moscow, PDR values in altitude (3–5 %) indicate the presence of a mixed elevated layer containing dust-like aerosols.

Between Krasnoyarsk and Nizhneudinsk, AOT values up to 0.28 have been observed, with a large fraction located in the free troposphere (up to 47 %). As they are associated with very low values of PDR (< 1 %), both below and above 1500 m a.g.l., it could either be pollution aerosols transported from the industrial city of Krasnoyarsk, or more probably part of a forest fire plume. Finally, small AOT values (below 0.1 at 355 nm) show that Russian background aerosols were sampled between Pskov and Smolensk (West of Moscow, not shown on Fig. 5), between Omsk and Novosibirsk, and in Istomino village, on the shore of Lake Baikal (between Irkutsk and Ulan-Ude).

3.3 Classification of boundary layer aerosols

Among the 193 profiles for which a BER could be retrieved, 69 (36 %) are located in Istomino village, on Lake Baikal shore, as several days of observations have been recorded there between 29 June and 7 July 2013. In order not to give the Baikal region an excessive weight, the BER distribution is computed on the 124 profiles recorded elsewhere than Istomino village (Fig. 6). BER values range from 0.006 to 0.045 sr^{-1}, which corresponds to lidar ratio values from 22 to 171 sr. The average BER during the campaign was 0.017 sr^{-1} (58 sr) with a SD of 0.009 sr^{-1} (± 41 sr) and a distribution that is clearly skewed towards small values (the median BER of 0.015 sr^{-1} being lower than the average). In Istomino village, the range of BER values is the same but the distribution (not shown) is shifted towards the higher values and slightly more scattered, with an average value and SD of 0.021 and 0.010 sr^{-1}, respectively.

Comparisons can be made with three aerosol classifications that provide BER values for different types of particles: (i) Cattrall et al. (2005) using sun-photometers from the AERONET network (BER at 550 nm), (ii) Burton et al. (2012) using high spectral resolution lidar observations from several campaigns over North America and the Caribbean (BER at 532 nm), and (iii) Müller et al. (2007) using a multi-wavelength N_2-Raman lidar on different sites over Europe and Asia (BER at 355 and 532 nm). The values obtained

ACPD
14, 27881–27944, 2014

during these previous studies and the comparisons with the work presented here are summarized in Tables 1–3. The campaign average BER ($0.017\,sr^{-1}$) exhibits a dominance of pollution or biomass burning aerosols (both having BER values standing from 0.014 to $0.019\,sr^{-1}$). The lower BER values in the left wing of the distribution are consistent with the 0.011 and $0.012 \pm 0.002\,sr^{-1}$ values observed in Paris by Raut and Chazette (2007) and Royer et al. (2011), indicating that those cases consist of pure pollution particles. BER values corresponding to desert dust aerosols ($> 0.019\,sr^{-1}$) are scarce in the general distribution while they are more frequent in Istomino village, where the average BER value ($0.021\,sr^{-1}$) indicates a dominance of dust-like aerosols.

To understand these results, it is necessary to keep in mind that these BER values are constrained in the lower PBL, implying that the elevated layers of dust or biomass burning aerosols have little influence. The relative weight given to the cities in the observations is increased thanks to the fixed night-time observations, but as most of the journey went through the rural, unpopulated areas of Siberia, the BER values represented in Fig. 6 stem from an average between pollution cases and remote background cases. Moreover, due to the terrigenous aerosols lifted from the ground, the BER values in Russian cities are likely to be higher than in European cities, where urban aerosols are dominated by carbonaceous particles from combustion processes.

To get more insight into the type of aerosols encountered, the scatter plot of PDR vs. BER values in the constraint layer (300–700 m a.g.l.) is presented on Fig. 7. Here, PDR values are computed from the profiles inverted with the campaign average BER, in order to prevent BER fluctuations from impacting the PDR. Of course, replacing the profile-constrained BER by the campaign average BER impacts the PDR value. To assess this effect, the 300–700 m average PDR was computed using either the constrained BER values or the average one. The distribution of PDR absolute difference (not shown here) is symmetric and centered around zero (the median is 4×10^{-3} %), indicating that the BER substitution does not introduce a systematic bias in the PDR values. For 50 % (resp. 90 %) of the profiles, the difference in PDR is lower than 0.2 %

ACPD
14, 27881–27944, 2014

(resp. 0.9 %), showing that the PDR values computed using the campaign average BER can be used to study the distribution along the journey.

Dots on Fig. 7 are colored according to their geographic origin. Aerosols from Europe (longitude < 26° E, red dots) are characterized by low BER and low PDR values (0.006 to 0.018 sr^{-1} and 0.5 to 1.3 %) indicating the predominance of carbonaceous particles. In Russia, profiles were split between urban and background cases, the "urban" criterion being a longitude difference smaller than 0.5° with the city center. Profiles were also split between the dust event zone (longitude from 45 to 75° E) and the rest of the country. Cities in the dust zone are Kazan, Ufa, Chelyabinsk and Omsk (Ishim is not included because too small); other Russian cities are Pskov, Moscow, Nizhniy-Novgorod, Novosibirsk, Irkutsk and Ulan-Ude (Nizhneudinsk is not included because too small). Krasnoyarsk was analyzed separately.

Russian cities (black and orange dots) show higher PDR values than European cities, all points except two being above 1.7 %. This is in accordance with our observations of the abundance of terrigenous aerosols being lifted from the cities surface. Krasnoyarsk is the only one city where PDR values are comparable with European cities but this is probably not due to a difference in the aerosol sources. Indeed, heavy rain had fallen during the night before the van went through the city and the ground was still wet, proving that the terrigenous aerosol had all been washed down. Cities located in the area where elevated layers of dust were observed (orange dots) do not show a different distribution of BER and PDR compared to other Russian cities (black dots). This indicates that the mixing of the elevated dust layers towards the PBL was low, or that its effects were limited as the BER values were already affected by terrigenous aerosols from local sources lifted in the PBL. Finally, the BER values in Russian cities are more variable than in European cities (from 0.006 to 0.035 sr^{-1}, except one outlier).

On the contrary, regarding the background profiles, there is a clear difference between profiles recorded in the area where elevated dust layers were observed, for which the 300–700 m average PDR values are all above 1.8 %, and the rest of the country, where PDR values are all below 1.3 %. Background aerosols in the unpop-

ACPD
14, 27881–27944, 2014

ulated areas of Russia result probably from a mixing between aged particles from biomass burning and secondary organic aerosols, so that very low depolarization can be expected when no dust is present. Also, under local terrigenous aerosol source-free conditions, the dust plume has a more sensible effect on the PDR than in town. BER values in remote areas are very variable (0.013 to 0.046 sr^{-1}). However, in the absence of dust, the AOT values used as constraint are small and result in large uncertainties on the BER values.

3.4 Temporal representativeness of the observations

To assess the representativeness of our measurements, the lidar-derived AOT presented in the previous section were compared with the optical thickness measured by MODIS Terra, using the monthly averaged and $1^{\circ} \times 1^{\circ}$ gridded product MOD08_M3. AOT from MODIS 412 nm channel was converted to AOT at the lidar wavelength using the monthly averaged Ångström coefficient between MODIS 470 and 660 nm channels. MODIS data from the grid pixel where the lidar was located were extracted and no spatial interpolation was performed. The months of June from years 2000 to 2013 (Terra launch to the campaign year) were then averaged; years when intense fire events occurred (2001, 2003 and 2012) were removed because they were not representative of the conditions experienced during the campaign.

The four AERONET stations located close to the path of the van (Palaiseau, Mainz, Moscow and Irkutsk) were also included in the comparison. The 380 nm sunphotometer AOT was converted to the lidar wavelength using the Ångström coefficient computed between the 380 and 440 nm channels (the 340 nm channel was not used as it can be biased at high solar zenith angles and high aerosol loads, Zhao et al., 2012). The monthly averages were computed from the daily averages including at least 4 observations, and the multi-annual June average was computed from years 2006 to 2013. The time period is different from MODIS because Mainz and Irkutsk stations do not have data prior to 2006. The resulting 355 nm AOT values for the lidar, MODIS and AERONET, are presented in Fig. 8 (top panel).

ACPD
14, 27881–27944, 2014

The lidar-derived AOT stays within a 1-σ interval around the MODIS multi-annual June average during most of the journey. The largest deviation from the average was observed between Ishim and Omsk, due to the mixed dust and biomass burning event identified in Sect. 3.1. However, the values of AOT (< 0.4) remain small compared to values observed during years of intense fires (MODIS monthly averaged AOT for June 2012 reaches up to 0.8 in the fire region). The pure dust layers observed near Kazan, as well as the fire or pollution layers observed near Nizhneudinsk are associated with moderate AOT values, which remain close to MODIS multi-annual June average. In the areas where we observed background aerosols, i.e. between Pskov and Smolensk ($\sim 30^\circ$ E, West of Moscow) and between Omsk and Novosibirsk ($\sim 80^\circ$ E), lidar AOT values are lower than 0.1 and clearly below MODIS. Therefore, the N_2-Raman lidar observations performed in Russia sampled both the clean background and dust and fire events that are not exceptional in amplitude and can then be considered representative of aerosols in remote parts of Siberia.

In the European part of the transect, AOT values observed by the lidar are close to MODIS multi-annual June average, except in Central Germany (Leipzig area) where lidar AOT values are clearly below MODIS. N_2-Raman lidar observations in Europe sampled both moderate pollution levels and background, and can also be considered representative of the aerosol load in June.

In middle and bottom panels of Fig. 8, the blue curves (green dots) present the 470–660 (440–675) nm Ångström coefficient and the 550 (500) nm AOT fine mode fraction from MODIS Terra (AERONET). The average and SD have been computed the same way as the AOT. These observations cannot be compared with the lidar but they underline an interesting transition around 23° E, i.e. where the van left Poland for Lithuania. There, MODIS shows a drop in AOT from an average of 0.2–0.3 in Europe to an average of 0.1–0.2 in the Baltic countries and Russia. This is correlated with an increase of the Ångström coefficient (0.8 to 1.4 in most Europe vs. 1.4 to 1.7 in Russia) and of the fine mode fraction (0.15 to 0.6 in Europe vs. 0.5 to 0.8 in Russia). This indicates that the aerosol mixture in Russia contains more small particles than in Eu-

ACPD
14, 27881–27944, 2014

rope. This fact would seem in contradiction with the observations of the N_2-Raman lidar showing that the aerosol mix over Russia includes a larger faction of coarse particles of terrigenous type.

In fact, this discrepancy is probably due to the differences in the observation scales. The BER and PDR values observed by the N_2-Raman lidar indicate the presence of coarse terrigenous aerosols, but these observations concern only the lower PBL (300–700 m a.g.l.) and the areas nearby the road followed by the van. In the lower PBL and near this road (one of the busiest of Russia), it is more likely to observe dust-like particles lifted by the wind or by the intense traffic which includes a large number of trucks. On the other hand, MODIS Ångström coefficients and fine mode fractions retrievals, that indicate the dominance of small particles over Russia, represent an average over the whole atmospheric column and a land surface of $1^\circ \times 1^\circ$ (111 km × 64 km at 55° N). MODIS observations are therefore more representative of the free troposphere and of the rural areas of Russia, where the aerosol mixture is dominated by biomass burning particles. In Moscow however, the city is large enough to occupy a significant part of the $1^\circ \times 1^\circ$ pixel and MODIS exhibits a drop of the fine mode fraction from 0.7 to 0.3 in this single pixel (the effect is lower on the Ångström coefficient though it slightly decreases).

The analysis of AERONET sun-photometers data along the journey shows a slight increase of the Ångström coefficient from Europe (Palaiseau and Mainz) to Russia (Moscow and Irkutsk) though this increase is much less pronounced than on MODIS observations. The fine mode fraction, however, does not exhibit any significant difference between Europe and Russia. This might be due to a difference between the models of aerosols used in AERONET and MODIS retrievals.

Finally, the dust event near Kazan is visible on MODIS daily gridded product (not shown here). It results in a zero small mode fraction and a 0.6 Ångström coefficient, values that are far from the multi-annual MODIS average. This shows that such a phenomenon is quite uncommon and confirms that the multi-annual average is dominated by biomass burning aerosols.

ACPD
14, 27881–27944, 2014

4 Characterization of dust and biomass burning aerosols events

This section presents case studies of dust or biomass burning aerosol plumes during which a finer characterization of the optical properties of these particles was possible. The origin of the particles is also studied for each plume. Finally, a comparison with observations made in other regions of the world is presented in Sect. 4.4.

4.1 Dust and biomass burning aerosols observed West of Kazan

The first significant observation of dust layers occurred near Kazan (49° E, 56° N). The weather was mostly overcast this day, so that only one hour and 45 min of cloudless observations could be recorded, starting ~ 35 km West of Kazan city. A map of the lidar 5 min average profile locations is presented on Fig. 9 along with MODIS Aqua Aerosol Optical Thickness (AOT, MYD04_L2 product). MODIS indicates moderate AOT values during Terra overpass at 07:30 UTC (AOT ~ 0.2, not shown here) but during Aqua overpass at 09:20 (Fig. 9), values have risen up to ~ 0.5, even 0.9 more to the West, showing the arrival of an aerosol plume. In the time interval between Aqua overpass and the lidar observations (~ 17:30 UTC), the wind blew from the south-southwest at the dust-like layer altitude, according to the reanalyzes from the European Center for Medium range Weather Forecast (ECMWF, ERA-Interim product at 0.75° and 6 h resolution). This direction is perpendicular to the AOT gradient visible on MODIS so it is possible to suppose that the general pattern in AOT was conserved until the van arrived.

4.1.1 Aerosol optical properties

The Backscatter to Extinction Ratio (BER) profile is computed on a 55 min average profile (17:29–18:24 UTC). Even after selecting only the data recorded after sunset (around 17:25 UTC), the signal to noise ratio (SNR) is close to its acceptable limit for inversion (~ 20) in the upper part of the profile. The profile is treated both using the Raman inversion (with a very wide filter due to the low SNR: parameters $a = 1$

ACPD
14, 27881–27944, 2014

and $b = 24$) and using the constrained Klett procedure on a sliding window as described in Sect. 2.2.4 (window width and shift of 200 m). The resulting extinction and BER profiles are presented on Fig. 10, along with the uncertainties computed through the Monte-Carlo process. The two inversions result in a very good agreement above 1.05 km a.m.s.l.; below this altitude, the constrained Klett procedure did not converge due to the low aerosol load.

The aerosol extinction coefficient profile shows the existence of four layers above 1.05 km a.m.s.l. (altitude above mean sea level). According to the particle depolarization profile (not shown here), the dust layer corresponds to the two highest layers and extends from 2.05 to 3.45 km a.m.s.l. With an average extinction of 0.05 km^{-1}, the lower part of the dust layer (2.05–2.85 km a.m.s.l.) is the denser of the two sub-layers. Both inversion processes agree on an average BER of $0.013 \pm 0.002\ sr^{-1}$ (75 ± 12 sr) in this sub-layer. Conversely, the upper part of the dust layer (2.85–3.45 km a.m.s.l.) has a much lower density, as the average extinction is only 0.03 km^{-1}. This results in large uncertainties on the BER values, both for the Raman inversion ($0.021 \pm 0.009\ sr^{-1}/48 \pm 25$ sr) and for the constrained Klett process ($0.023 \pm 0.012\ sr^{-1}/43 \pm 32$ sr). In the literature, the experimental BER values associated with dust layers are very variable (see Table 1) and will be discussed thoroughly in Sect. 4.4.1. Still, we note that the 0.013 sr^{-1} BER value retrieved in the Kazan lower dust layer corresponds to the lowest limit of the results reported in literature (Mattis et al., 2002) while the 0.022 sr^{-1} BER value retrieved in the Kazan upper dust layer is more within the range of other observations (e.g. Burton et al., 2012) though it is marred by a large uncertainty.

A finer temporal sampling can be considered using the 5 min average profiles. Hence, the inversion is performed using the BER profile derived from the constrained Klett procedure. The resulting aerosol extinction coefficient and Particle Depolarization Ratio (PDR) are presented on Figs. 11 and 12. The PDR clearly highlights the presence of a dust layer in altitude, with an average value of 23 % from 17:15 to 17:45 UTC and between 2.05 and 2.85 km a.m.s.l. (lower part of the layer) and 20 % between 2.85 and 3.45 km a.m.s.l. (upper part of the layer). The temporal and spatial variability of the

ACPD
14, 27881–27944, 2014

PDR inside the layers is the dominant source of uncertainty (± 2 %). Values of desert dust PDR reported in the literature are also very variable (see Table 1) and depend whether the dust layer is pure or mixed with another type of aerosol with lower intrinsic depolarization power (i.e. pollution or biomass burning aerosols). The detailed discussion about dust layers PDR values will follow in Sect. 4.4.1. We can partially conclude that the plume observed west of Kazan certainly contains dust particles, relying on the fact that the PDR is 23 %. Nevertheless, it is difficult to determine whether it is pure, especially as dust in southern Russia is not originated from sources that have been previously described in the literature.

The aerosol extinction coefficient plot (Fig. 11) also shows a dense layer between 0.95 and 1.55 km a.m.s.l. that corresponds to the lowest visible layer on the average extinction coefficient profile (Fig. 10, left). The average BER value associated to this layer is low using both retrievals: $0.010 \pm 0.002\,sr^{-1}$ (i.e. a LR of 104 ± 21 sr). The PDR also is very low (Fig. 12) with an average value of 1.9 % in the densest part of the layer (before 17:00 UTC and between 1.05 and 1.25 km a.m.s.l.). Here, the uncertainty calculated from the Monte-Carlo process is lower than 0.1 % but the time and space variabilities in the layer are very large (± 1.1 %). Based on these elements, we can conclude that we are facing a case of biomass burning layer (see references in Table 2 and detailed discussion in Sect. 4.4.2). Indeed, pollution particles are very unlikely as the wind was not coming from Kazan or Nizhniy-Novgorod, which are the only large cities in the region.

4.1.2 Origin of the dust particles

To identify the dust sources, Fig. 13 presents 7 day backward trajectories from the Hybrid Single Particle Lagrangian Integrated Trajectory Model (HYSPLIT 4) in ensemble mode (the wind field at the ending point is shifted by one grid point to assess the effect of uncertainties on the wind). The back-trajectories have been calculated under the isentropic mode for the vertical velocity. The ending point was chosen in the dust layer, (2.6 km a.m.s.l.), above the lidar location at 17:00 UTC. As 20 trajectories out of

ACPD
14, 27881–27944, 2014

27 did not touch ground during their journey, most of the air mass was originated from the free troposphere, so that the dust concentration was probably low, explaining the low aerosol extinction coefficient. Among the 7 remaining trajectories, ground contact occurred in the North-Western and central parts of Kazakhstan, in the Volga mouth region and in the area between the Caspian and Aral seas.

The maps of aerodynamic roughness lengths established using the ERS scatterometer (Pringent et al., 2005) or the ACAST and PARASOL instruments (Pringent et al., 2012) show values of roughness length between 0.02 and 0.04 cm in the Aral-Caspian region, and 0.04 to 0.08 cm in all the Northern part of Kazakhstan. Geological maps available from the European Soil Portal (http://eusoils.jrc.ec.europa.eu/library/esdac/index.html) show that large sandy areas stand at the South and East of the Aral Sea (Kyzylkum and Karakum deserts), and to a lesser extent at the North-West of the Caspian Sea. In the area between the Aral and Caspian seas, and also in large parts of central Kazakhstan, soils are of loamy type, even including clay deserts ("takyr") or salt deserts ("solonchak"). Conditions for dust lifting by saltation are thus gathered in this region, as it offers sources of large particles (saltators) whose impact on the ground can splash away the smaller clay particles then able to undergo long range transport.

4.2 Dust and biomass burning aerosols observed above Omsk

Omsk is one of Russia's largest industrial centers and a 1.15 million inhabitant city located 2300 km East of Moscow (55° N, 73° E). Several oil and gas fields are exploited north of the city, whose industry is dominated by gas and oil manufacturing (the largest petrochemical complex of Russia is located near Omsk). The van was stationed in the center of the city, near the Irtysh River, during the night of 22–23 June.

4.2.1 Aerosol optical properties

Observations show the successive overpass of a dust layer and a biomass burning layer over the van. To determine the BER, two average profiles were computed:

ACPD
14, 27881–27944, 2014

one that samples the overpass of the dust layer (16:44–19:12 UTC) and one during the overpass of the biomass burning layer (19:12–21:42 UTC). Both profiles include only nighttime data (sunset/sunrise at 15:50/22:30 UTC) so that the N_2-Raman signal reaches the molecular zone (> 4 km). Figure 14 presents the BER profiles computed using the Raman inversion (filter parameters $a = 1$ and $b = 15$) and the constrained Klett inversion (window width and shift of 250 m).

In the heart of the dust layer (left profile, 2.5–3.5 km a.g.l.), the average BER is $0.020 \pm 0.003\,sr^{-1}$ according to the constrained Klett inversion and $0.023 \pm 0.004\,sr^{-1}$ according to the Raman inversion (44 ± 8 sr). These BER values are in the average of what is reported in the literature for desert dust aerosols (see references in Table 1 and detailed discussion in Sect. 4.4.1). Contrary to what has been observed for the dust layer near Kazan, no smoke layer is present just below the Omsk dust layer. Therefore, a mixing with biomass burning aerosols is less likely and BER values observed over Omsk can safely be attributed to pure dust. In the biomass burning layer that arrived later in the night (right profile, 1.5–2.5 km a.g.l.), both inversion methods lead to an average BER of $0.013 \pm 0.002\,sr^{-1}$ (76 ± 12 sr), a value that falls in the lower range of what is reported in the literature for biomass burning aerosols (see Table 2 and discussion in Sect. 4.4.2).

In the residual layer (0.5–1.0 km a.g.l.), BER values seem to decrease slightly during the night: before 19:00 UTC (profile #1), the average BER is $0.013 \pm 0.002\,sr^{-1}$ for the constrained Klett inversion and $0.014 \pm 0.003\,sr^{-1}$ for the Raman inversion (70 ± 12 sr), while after 19:00 UTC (profile #2), the average BER is only 0.010 ± 0.001 and $0.011 \pm 0.002\,sr^{-1}$ for the Klett/Raman inversions respectively (95 ± 16 sr). However, it is difficult to assess whether this decrease in BER is significant as the associated error bars are not fully separated. In the literature (Table 3), BER values for pollution aerosols range between $0.011 \pm 0.002\,sr^{-1}$ (Raut and Chazette, 2007) and $0.017 \pm 0.004\,sr^{-1}$ (Müller et al., 2007), both at 355 nm. Burton et al. (2012) give a 0.014–0.019 sr^{-1} interval in their aerosol classification. The values that we observed in the Omsk residual layer are therefore in the lower end of the observation range. Fi-

ACPD
14, 27881–27944, 2014

nally, BER values above 3.9 km and between 1.1 and 1.4 km a.g.l. are not significant due to the very low aerosol load.

To invert the aerosol extinction coefficient, the BER profiles retrieved from the constrained Klett inversion process are used (only the uppermost layer is removed as the BER did not converge at the limit of the molecular zone); a linear transition is introduced between 18:55 and 19:30 UTC in order to avoid a discontinuity in time. The average aerosol extinction coefficient is only $0.02 \pm 0.01\,km^{-1}$ in the dust layer (16:44–19:12 UTC, 2.5–3.3 km a.g.l.), against $0.09 \pm 0.03\,km^{-1}$ in the smoke layer (19:12–22:30 UTC, 1.4–2.6 km a.g.l.). Figure 15 also shows a large decrease in the extinction coefficient between the late afternoon turbulent boundary layer (14:33–15:30, 0.3–1.2 km a.g.l., average extinction of $0.122 \pm 0.017\,km^{-1}$) and the residual layer (19:12–22:30, 0.3–1.0 km a.g.l., average extinction of $0.039 \pm 0.008\,km^{-1}$) following the disconnection from fresh ground emissions. After 18:00 UTC, the biomass burning and residual layers were separated by a clean layer associated with a sharp wind shear visible between the 900 and 850 hPa levels on the ECMWF ERA-Interim reanalysis (not shown here).

The AOT (Fig. 15, upper panel) decreased from ~ 0.27 during late afternoon to ~ 0.17 at 19:00 UTC, mainly due to the decrease of extinction in the residual layer after sunset. After 19:00 UTC, AOT rose again due to the arrival of the biomass burning layer. MODIS observations show that the dust and biomass burning plume was already present the previous morning during Terra and Aqua overpasses (22 June ~ 07:00 UTC). The very high 355 nm AOT values (~ 0.7) suggest that the plume was denser at this earlier moment and that the lidar observations sampled only the edge of the plume. This is confirmed by the overpass of MODIS Terra on 23 June (06:10 UTC) which produces an AOT value similar to the lidar observations 5 h earlier (AOT ~ 0.17).

The particle depolarization ratio (Fig. 16) displays the reverse pattern of the aerosol extinction coefficient. Indeed, the dust and biomass burning layers stand out with an average PDR of 16 ± 2 % and 3.5 ± 1.6 %, respectively. In the most depolarizing part of the dust layer (15:45–16:17 UTC, 2.8–3.2 km a.g.l.), the PDR even reaches 21 ± 4 %.

ACPD
14, 27881–27944, 2014

Such a value is similar to the observations near Kazan and appeals the same discussion as in Sect. 4.1.1: knowing whether this layer is pure desert dust or a mix with other types of aerosols is not possible given the PDR values reported in the literature (Table 1, Sect. 4.4.1). Finally, below 1 km a.g.l., there is little change in depolarization between the afternoon turbulent boundary layer (3.8 ± 0.5 %) and the residual layer (3.2 ± 0.8 %). Both values are compatible with the classification of Burton et al. (2012), who reported 3 to 8 % of depolarization for pollution aerosols, and with the observations of Müller et al. (2007), who always observed PDR values lower than 5 % for urban haze.

4.2.2 Origin of the elevated layers

Figure 17 displays HYSPLIT 7 day back-trajectories ending in the dust layer above Omsk. These trajectories show many changes of direction or even cusps, except during the last two days when they all converged in a North-West/South-East turn. Examination of the geopotential height maps extracted from ECMWF reanalyzes (not displayed here) show that the air mass was close to the center of a high pressure system from 15–19 June, so that the weak and changing winds produced erratic trajectories. When the anticyclone strengthened and moved north-east, on 20 June, the air mass started curling around it and quickly reached Omsk.

Due to wind shear, the back-trajectories split into three families: the first one had ground contact in the region located east of Chelyabinsk and Yekaterinburg (~ 64° E), a region composed of forests and grasslands. The two other families of back-trajectories touched ground more to the West, in a wide area standing from the Ufa region (55° N, 56° E) to the Aral Sea. The desert dust plume observed above Omsk thus has the same origin as the layer observed near Kazan 5 days earlier, i.e. the sandy/loamy soils of south-western Kazakhstan. Actually, the high pressure system that drove dust from Kazakhstan above Omsk is the same that brought it above Kazan and Ishim and even Moscow (these two latter cases are not detailed). This anticyclone detached itself from a larger high pressure system located over Europe around 14 June

ACPD
14, 27881–27944, 2014

and then moved eastwards along with the lidar van until 22 June, when it took another direction than the van trajectory and departed northwards. As the winds curled around the anticyclone, air masses which had passed over the dust source region were continuously brought up to the North, producing dust outbreaks over 2300 km, from Moscow (38° E) to Omsk (73° E).

The back-trajectories (not shown here) ending above Omsk a few hours later, during the overpass of the biomass burning layer are very similar to those presented on Fig. 17 due to the stable anticyclonic weather situation. The back-trajectories pass at low altitude above three fire areas highlighted by MODIS Terra on 18 and 19 June and located in the steppes of north-western Kazakhstan (51° N–54° E, 50° N–56° E and 48° N–57° E). Their fire radiative power was between 90 and 120 MW according to the MODIS product from the University of Maryland (MCD14ML; Giglio et al., 2006). Fires hot-spots were also observed by MODIS in the wooded area corresponding to the latest part of the back-trajectories (60–62° N, 69–73° E) and from 17–25 June at least. However, as the fire radiative power is low (max. 38 MW), the injection height might not be large enough to allow the aerosols to catch up with the air mass that, according to HYSPLIT, passed above this region above 2 km a.g.l. On the other side, those fires were detected at the edge of a cloud system, suggesting that other fire areas with higher fire radiative power, thus higher injection heights, might have existed further north and escaped detection by MODIS.

4.3 Additional cases

Some additional cases that cannot be detailed extensively will be briefly described in this section; results are summarized in Tables 1 and 2.

During the night from 21–22 June, the van stopped near the town of Ishim (65 000 inhabitants, 56° N, 69° E). A small depolarizing layer is observed between 1.2 and 1.7 km a.g.l. at the start of the record. This layer's BER can be determined from a 50 min average profile, using the sliding-window constrained Klett procedure (window width and shift of 300 m). The BER in the layer is $0.011 \pm 0.005\,sr^{-1}$ (90 ± 12 sr), a value

ACPD
14, 27881–27944, 2014

close to the $0.013 \pm 0.002\,sr^{-1}$ observed 4 days earlier in the lower part of Kazan dust layer. The PDR is $15 \pm 2\,\%$, i.e. closer to the $16 \pm 2\,\%$ observed in Omsk dust layer on the day after. HYPSLIT back-trajectories (not shown) confirm that these dust particles have the same origin that those observed near Kazan and Omsk.

A biomass burning layer was also observed above Ishim during the second part of the night, between 0.6 and 2.1 km a.g.l. The BER can be determined from a 1 h and 40 min average profile, using the complete Raman inversion ($a = 1$, $b = 19$). The average BER in this layer is $0.015 \pm 0.001\,sr^{-1}$ ($67 \pm 3\,sr$) and the PDR is $3.2 \pm 0.2\,\%$, i.e. values close to what was observed in Omsk biomass burning layer on the following night. In the residual layer, the BER is much higher: $0.026 \pm 0.002\,sr^{-1}$ ($39 \pm 3\,sr$), reflecting the dominance of terrigenous aerosols in this small city where the industrial activity is mainly food-processing.

During the night from 25–26 June, the van halted in the small city of Nizhneudinsk (55° N, 99° E, 37 000 inhabitants). No dense layers of aerosols were visible but a diffuse background reached up to 3.5 km a.g.l. Using a full Raman inversion ($a = 1$, $b = 19$) on a 1 h and 20 min average profile, the BER of this background is found to be $0.014 \pm 0.002\,sr^{-1}$ ($70 \pm 9\,sr$) while its PDR is $0.9 \pm 0.2\,\%$. Back-trajectories (not shown here) show that the air mass came from the Far North but a dense cloud cover blinded MODIS and prevented the identification of the aerosol sources.

Dust plumes were also visible while the van traveled in between cities although daytime observations do not allow the quantitative determination of the BER and PDR for elevated layers. Those cases will therefore not be included in the discussion.

4.4 Discussion

To synthesize, BER and PDR values from the different case studies are summarized in the lower part of Table 1 (desert dust) and Table 2 (biomass burning), along with the references they can be compared with.

ACPD
14, 27881–27944, 2014

4.4.1 Desert dust

Particle depolarization ratio. High values of the particle depolarization ratio are the most certain way to identify desert dust layers, as only volcanic ash can exhibit such high PDR values (Chazette et al., 2012). The depolarization ratios observed for desert dust during the campaign vary between 15 and 23 % (Table 1, lower part). They are in fairly good agreement with previous observations also made at 355 nm. Indeed, Tesche et al. (2011) observed similar PDR values at 355 nm in Saharan dust layers advected over Morocco and Cape Verde during the Saharan Mineral dust experiments (SAMUM): they reported 26 ± 6 % for pure dust and 16 ± 4 % for a mix of dust and biomass burning. Chazette et al. (2014) found lower PDR values at 355 nm, between 16 and 19 %, in Saharan dust layers advected over the Balearic Islands during the Hydrological cycle in Mediterranean Experiment (HyMeX) campaign. Based on observations from 14 airborne campaigns over North America and the Caribbean, Burton et al. (2012) reported 532 nm PDR values ranging from 30 to 35 % for pure dust layers, and from 10 to 28 % for dust mixed with pollution or biomass burning (what they called "dusty mix"). Tesche et al. (2011) presented simultaneous observations at 355, 532 and 710 nm and showed that the PDR of desert dust increases with wavelength. They reported values of 31 ± 3 % at 532 nm that are similar to the observations of Burton et al. (2012). Therefore, it is not surprising to have less agreement with observations of depolarization ratio made at higher wavelengths.

Backscatter to extinction ratio. The BER values reported in the literature for pure desert dust are very variable and range from 0.013 to 0.029 sr^{-1} (34–77 sr, see Table 1, upper part). The aerosol classification based on AERONET sun-photometers spread all around the world gives an average BER value of 0.024 ± 0.002 sr^{-1} (42 ± 4 sr) at 550 nm (Cattrall et al., 2005) while the aerosol classification based on airborne high spectral resolution lidar data recorded over North America and the Caribbean gives BER values ranging from 0.018 to 0.024 sr^{-1} (42–56 sr) at 532 nm (Burton et al., 2012). Note that observations with a multi-wavelength N_2-Raman lidar (at 355 and 532 nm)

ACPD
14, 27881–27944, 2014

showed that the BER of desert dust particles does not vary much with wavelength (Müller et al., 2007; Murayama et al., 2004; Tesche et al., 2011). Therefore, observations at 532 nm can be directly compared to the results from our study.

Among all deserts, the Saharan desert dust is probably the best documented, as several campaigns produced observations using N_2-Raman lidars. Tesche et al. (2011) reported an average BER of $0.019 \pm 0.003\,sr^{-1}$ (53 ± 10 sr) at 355 nm for dust advected over Cape Verde during SAMUM. Chazette et al. (2014) found similar 355 nm BER values, from 0.016 to $0.021\,sr^{-1}$ (48–63 sr), for dust advected over the Balearic Islands during HyMeX. Further south, Chazette et al. (2007) reported a higher BER value of $0.025 \pm 0.006\,sr^{-1}$ (40 ± 11 sr), also at 355 nm, in the Harmattan layer over Niamey (Niger) during AMMA. On the contrary, (Mattis et al. (2002) found slightly lower BER values at 532 nm, from 0.013 to $0.020\,sr^{-1}$ (50–77 sr), in the case of aged Saharan dust advected over Germany. Elsewhere, Arabian dust advected over the Maldives Islands and observed during INDOEX had an average BER of $0.026 \pm 0.004\,sr^{-1}$ (38 ± 6 sr; Müller et al., 2007) at 355 nm. Closer to southern Russia, Asian dust from China (Gobi desert) were associated with a high BER of $0.029 \pm 0.004\,sr^{-1}$ (34 ± 5 sr) at 355 nm in a layer advected over Beijing (Müller et al., 2007) though the 355 nm BER was only of $0.020 \pm 0.004\,sr^{-1}$ (50 ± 11 sr) in a layer advected over Tokyo (Murayama et al., 2004).

In the case of desert dust mixed with biomass burning aerosols or pollution, Burton et al. (2012) also reported very variable BER values at 532 nm, ranging from 0.016 to $0.067\,sr^{-1}$ (16–63 sr) though the most frequent values ranged only from 0.024 to $0.033\,sr^{-1}$ (30–42 sr) vs. 0.020 to $0.023\,sr^{-1}$ for pure dust. This view seems counter intuitive as it means that the BER values tend to increase when the dust is mixed with aerosols of higher absorbing power (that have a higher extinction coefficient). The opposite effect, and more logical according to us, was observed at 355 nm for mixed layers containing both Saharan dust and smoke from forest fires in West Africa: Tesche et al. (2011) reported an average BER of $0.015 \pm 0.003\,sr^{-1}$ (67 ± 14 sr) for the aerosol mix vs. $0.019 \pm 0.003\,sr^{-1}$ for pure dust. Similarly, Chazette et al. (2007) found a value of $0.015\,sr^{-1}$ for the aerosol mix vs. $0.025\,sr^{-1}$ for pure dust. Observations performed

ACPD
14, 27881–27944, 2014

with a multi-wavelength N_2-Raman lidar (at 355 and 532 nm) showed that, unlike desert dust aerosols, the BER value of biomass burning aerosols can vary significantly with wavelength (Müller et al., 2005; Murayama et al., 2004; Nicolae et al., 2013; Tesche et al., 2011). Moreover, these studies disagree on the way the BER varies with wavelength, therefore, it is safer to limit the comparison to the observations made at the same wavelength as in this study (Chazette et al., 2007; Tesche et al., 2011) and consider that the BER decreases in the case of a "dusty mix".

In this perspective, the layer observed above Ishim, with a very low BER (0.011 sr^{-1}) and moderate PDR (15 %), is clearly a mix between desert dust and carbonaceous aerosols, most probably biomass burning from forest fires. The layer observed above Omsk and the upper part of the layer observed West of Kazan have BER values that are typical of dust (0.022 to 0.023 sr^{-1}) and also higher PDR values (20 to 21 %) that could fit with pure desert dust aerosols. The lower part of the layer observed West of Kazan has a 23 % PDR pointing toward pure desert dust but a 0.013 sr^{-1} BER that suggests a mixing with biomass burning aerosols. However, it is not possible to confirm whether what we observed was pure or mixed desert dust because, in both cases, biomass burning layers were observed close (in time or space) to the dust layer, and also because MODIS showed the presence of forest or grassland fires in the area where the air mass was supposed to came close to the ground level according to HYSPLIT. Actually, MODIS highlighted the regular presence of small to medium size fires over western Kazakhstan during the whole period immediately prior to the sampling and while the van journeyed north of this region (15–23 June). This means that the longer the air mass stayed in this region and the more spread out the back-trajectories are, the more likely it is that the dust got mixed with biomass burning aerosols. This is the case for the layers observed above Kazan and Omsk (Figs. 13 and 17) as well as Ishim (not shown).

ACPD
14, 27881–27944, 2014

4.4.2 Biomass burning

Particle depolarization ratio. PDR values for biomass burning layers observed in Siberia vary between 0.9 and 3.5 %. The lowest value was not observed in a dense layer, but in the diffuse particle background above Nizhneudinsk. It is also the only case where particles came from the Far North; during the three other biomass-burning events, the particles came from the steppes or forests of southern Russia and Kazakhstan. Unfortunately, the back-trajectories ending over Nizhneudinsk (not shown) passed in a zone of dense cloud cover so that it was not possible to identify precisely the origin of the particles through the MODIS fire product. The second lowest value (1.6 %) was observed in a thin layer (∼ 250 m deep) just at the boundary layer top, so the smoke plume might have been diluted during transport. In both cases when a thick and dense smoke layer was observed, the PDR is close: 3.2 % (Ishim) and 3.5 % (Omsk).

In the literature, depolarization ratios for aged smoke are 4–9 % (Burton et al., 2012), 5 ± 2 % (Tesche et al., 2011) or < 5 % (Müller et al., 2007), for measurements all performed at 532 nm. No simultaneous observations of PDR at 355 and 532 nm exist for biomass burning aerosols, although measurement of a mixed smoke and dust layer suggest that the PDR does not vary much with wavelength (Tesche et al., 2011). Therefore, observations in thick, dense layers (Ishim and Omsk) are in good agreement with the literature. The small layer above Kazan stands not so far from the extreme low (5th percentile at 2 %) given by Burton et al. (2012). However, the diffuse background of particles above Nizhneudinsk has a lower depolarization ratio than every observations reported. The low value of extinction in this diffuse background indicates that the particle concentration is small, suggesting that, rather than the plume from a single large fire, this might result from a mix between smoke from several small scattered fires and biogenic aerosols (secondary organics) collected all along the air mass journey over the plains of northern Siberia.

Backscatter to extinction ratio. BER values reported in the literature for aged biomass burning aerosols split into two families. The first one encompasses studies that re-

ACPD
14, 27881–27944, 2014

trieved low BER values, close to those of pollution aerosols (Table 3). This is the case in the aerosols classification based on worldwide ARONET sun-photometers (Cattrall et al., 2005) that reported an average BER value of $0.017 \pm 0.002\,sr^{-1}$ (59 ± 7 sr) at 550 nm. Similarly, the classification based on multi-campaign high spectral resolution lidar observations over North America and the Caribbean (Burton et al., 2012) reported values ranging from 0.012 to $0.022\,sr^{-1}$ (45–83 sr), most values being between 0.014 and $0.018\,sr^{-1}$ (56–71 sr) at 532 nm. The lowest BER values were observed using N_2-Raman lidars at 355 nm, in smoke plumes from fires in West Africa advected over Cape Verde during SAMUM ($0.011 \pm 0.003\,sr^{-1}$ i.e. 91 ± 27 sr; Tesche et al., 2011) or over Niger during AMMA ($\sim 0.009\,sr^{-1}$ i.e. 111 sr; Chazette et al., 2007).

Another family of studies retrieved higher BER values, closer to those of desert dust aerosols (Table 1). Murayama et al. (2004) found a BER of $0.025\,sr^{-1}$ (40 sr) at 355 nm in a biomass burning layer advected over Tokyo from Siberia. Müller et al. (2005) reported $0.022 \pm 0.006\,sr^{-1}$ (45 ± 14 sr) at 355 nm in smoke plumes from Canada and Siberia advected over Germany. And Nicolae et al. (2013) retrieved BER values ranging from 0.02 to $0.031\,sr^{-1}$ (32–50 sr) at 355 nm in four fire plumes advected over Romania from Turkey, Ukraine and Southern Russia. Observations with a multi-wavelength N_2-Raman lidar (at 355 and 532 nm) showed a strong variability of the BER of biomass burning aerosols with wavelength (Müller et al., 2005; Murayama et al., 2004; Nicolae et al., 2013; Tesche et al., 2011) but even considering only observations made at the same 355 nm wavelength as in this study, BER values reported in the literature still split into pollution-like and dust-like families. This discrepancy in BER values might come from differences in the vegetation nature or in the soil type (as dust will be lifted from the nearby ground by the eddies caused by the fire heat); however, investigating the origin of this BER variability is out of the scope of this paper. We can only conclude that the BER values of biomass burning layers observed in Siberia during this campaign clearly belong to the first family of observations (pollution-like BER) as they range only from 0.010 to $0.015\,sr^{-1}$, and with little uncertainty (Table 2, lower part).

ACPD
14, 27881–27944, 2014

5 Conclusions

For one full month, a mobile N_2-Raman and depolarization lidar probed aerosols along the 10 000 km ride from Paris to Ulan-Ude (2 to 108° E). A systematic data-processing was performed on the 30 min average profiles: the Raman channel was used to constrain the inversion and determine the average backscatter-to-extinction ratio (BER) between 300 and 700 m a.g.l. The campaign average BER was found to be 0.017 sr^{-1} along the journey, and 0.021 sr^{-1} in the isolated village of Istomino (Lake Baikal shore). The distribution of the BER and particle depolarization ratio (PDR) values show that aerosols in Europe are characterized by low BER values (< 0.018 sr^{-1}) and low PDR (< 1.3 %) both in cities and in the countryside, indicating the dominance of pollution aerosols. In Russia, the BER values are much more variable (up to 0.046 sr^{-1}) and a clear distinction exists between the countryside, where the PDR is as low as in Europe (< 1.3 %), and the cities where the PDR is higher (> 1.7 %). The higher depolarization in Russian cities is likely due to the significant amount of terrigenous aerosols lifted by vehicles or by the wind from the roads and sidewalks that generally have a bad tarmac.

Fixed measurements were performed in the cities where the van carrying the lidar stopped for the night. Long time-averages enabled the determination of BER profiles above the cities through a complete Raman inversion using a low-pass derivative filter. The precise determination of the BER also enables an accurate retrieval of the PDR. Several events of biomass burning plumes were recorded during these nighttime observations, with BER values ranging from 0.010 to 0.015 sr^{-1} and PDR values of from 2 to 3 %. Desert dust layers were also observed, with BER (PDR) values around 0.022 sr^{-1} (21 %) for pure dust layers and 0.011 sr^{-1} (15 %) for a mixed dust and biomass burning layer. The back-trajectories analysis identifies the dust source in the region of the Caspian and Aral seas (south-western Kazakhstan), an area whose dust emissions had not been characterized so far. Moreover, dust layers were observed from Moscow to Omsk (37–73° E, ∼ 2300 km), demonstrating that the Caspian-Aral region can give

ACPD
14, 27881–27944, 2014

birth to large dust events spreading over wide areas of Russia and lasting for several days. Such an event does not require special conditions but a regular anticyclone moving eastwards over southern Russia or northern Kazakhstan, meaning such dust spreading could happen regularly and contribute significantly to the aerosol budget in southern Russia.

This ground-based mobile campaign provided a unique picture of summer aerosols in areas where observations are usually scarce. Although it was only a snapshot and not a climatology, these observations hold more representativeness for two reasons: first, the lidar instrument involved in this campaign enabled the determination of two intensive properties of the particles (BER and PDR) that do not depend on the aerosols amount. And secondly, the comparison with a multi-annual average of MODIS Terra observations showed that the AOT values observed during the campaign are representative of the aerosol loads existing over Europe and Russia in the absence of exceptional fire events like the ones that occurred in 2003 or 2010. Only the area where the dust event took place stands out from MODIS multi-annual average, however, it offered the opportunity to characterize the unstudied desert dust from the Caspian-Aral region.

Regarding the anthropogenic sources, a second paper is in preparation to present case studies of pollution hotspots along the journey and analyze in more details the variability of pollution aerosols optical properties in Europe and Russia. Then, future work will focus on identifying the frequency, geographical extent and duration of desert dust events such as the one observed during this campaign, using the space-borne observations from MODIS and CALIPSO. In a second step, radiative modeling studies can be conducted to assess the radiative impact of desert dust over southern Russia.

Acknowledgements. The authors would like to thank Frederik Paulsen, Honorary Consul for the Russian Federation in the canton of Vaud, Switzerland, both for his financial support and for getting the permission to operate in Russia. The authors are also very grateful to Alexander Ayurzhanaev from the Siberian Branch of the Russian Academy of Sciences, Laboratory of Physics of Atmospheric Processes, Ulan-Ude, for his vital help with the logistic of the journey while he was aboard the van. Finally, the authors thank Cyril Moulin, head of the Laboratoire des

ACPD
14, 27881–27944, 2014

Sciences du Climat et de l'Environnement, for his support and assistance in the administrative part of the project.

References

Ångström, A.: The parameters of atmospheric turbidity, Tellus, 16, 64–75, doi:10.1111/j.2153-3490.1964.tb00144.x, 1964.

Ansmann, A., Riebesell, M., and Weitkamp, C.: Measurement of atmospheric aerosol extinction profiles with a Raman lidar, Opt. Lett., 15, 746–748, doi:10.1364/OL.15.000746, 1990.

Bates, T. S., Huebert, B. J., Gras, J. L., Griffiths, F. B., and Durkee, P. A.: International Global Atmospheric Chemistry (IGAC) Project's First Aerosol Characterization Experiment (ACE1): overview, J. Geophys. Res., 103, 16297, doi:10.1029/97JD03741, 1998.

Burton, S. P., Ferrare, R. A., Hostetler, C. A., Hair, J. W., Rogers, R. R., Obland, M. D., Butler, C. F., Cook, A. L., Harper, D. B., and Froyd, K. D.: Aerosol classification using airborne High Spectral Resolution Lidar measurements – methodology and examples, Atmos. Meas. Tech., 5, 73–98, doi:10.5194/amt-5-73-2012, 2012.

Cattrall, C., Reagan, J., Thome, K., and Dubovik, O.: Variability of aerosol and spectral lidar and backscatter and extinction ratios of key aerosol types derived from selected Aerosol Robotic Network locations, J. Geophys. Res., 110, D10S11, doi:10.1029/2004JD005124, 2005.

Chazette, P.: The monsoon aerosol extinction properties at Goa during INDOEX as measured with lidar, J. Geophys. Res., 108, 4187, doi:10.1029/2002JD002074, 2003.

Chazette, P., Randriamiarisoa, H., Sanak, J., Couvert, P., and Flamant, C.: Optical properties of urban aerosol from airborne and ground-based in situ measurements performed during the Etude et Simulation de la Qualité de l'air en Ile de France (ESQUIF) program, J. Geophys. Res., 110, 2206, doi:10.1029/2004JD004810, 2005.

Chazette, P., Sanak, J., and Dulac, F.: New approach for aerosol profiling with a lidar onboard an ultralight aircraft: application to the African Monsoon Multidisciplinary Analysis, Environ. Sci. Technol., 41, 8335–8341, doi:10.1021/es070343y, 2007.

Chazette, P., Raut, J.-C., Dulac, F., Berthier, S., Kim, S.-W., Royer, P., Sanak, J., Loaëc, S., and Grigaut-Desbrosses, H.: Simultaneous observations of lower tropospheric continental aerosols with a ground-based, an airborne, and the spaceborne CALIOP lidar system, J. Geophys. Res., 115, D00H31, doi:10.1029/2009JD012341, 2010.

ACPD
14, 27881–27944, 2014

Chazette, P., Dabas, A., Sanak, J., Lardier, M., and Royer, P.: French airborne lidar measurements for Eyjafjallajökull ash plume survey, Atmos. Chem. Phys., 12, 7059–7072, doi:10.5194/acp-12-7059-2012, 2012.

Chazette, P., Marnas, F., and Totems, J.: The mobile Water vapor Aerosol Raman LIdar and its implication in the framework of the HyMeX and ChArMEx programs: application to a dust transport process, Atmos. Meas. Tech., 7, 1629–1647, doi:10.5194/amt-7-1629-2014, 2014.

Chi, X., Winderlich, J., Mayer, J.-C., Panov, A. V., Heimann, M., Birmili, W., Heintzenberg, J., Cheng, Y., and Andreae, M. O.: Long-term measurements of aerosol and carbon monoxide at the ZOTTO tall tower to characterize polluted and pristine air in the Siberian taiga, Atmos. Chem. Phys., 13, 12271–12298, doi:10.5194/acp-13-12271-2013, 2013.

Deuzé, J. L., Bréon, F.-M., Devaux, C., Goloub, P., Herman, M., Lafrance, B., Maignan, F., Marchand, A., Nadal, F., Perry, G., and Tanré, D.: Remote sensing of aerosols over land surfaces from POLDER-ADEOS-1 polarized measurements, J. Geophys. Res., 106, 4913–4926, doi:10.1029/2000JD900364, 2001.

Ferrare, R. A., Melfi, S. H., Whiteman, D. N., Evans, K. D., and R, L.: Raman lidar measurements of aerosol extinction and backscattering, 1. Methods and comparisons, J. Geophys. Res., 103, 19663–19672, doi:10.1029/98JD01646, 1998.

Giglio, L., Csiszar, I., and Justice, C. O.: Global distribution and seasonality of active fires as observed with the Terra and Aqua Moderate Resolution Imaging Spectroradiometer (MODIS) sensors, J. Geophys. Res., 111, 2016, doi:10.1029/2005JG000142, 2006.

Holben, B. N., Eck, T. F., Slutsker, I., Tanré, D., Buis, J. P., Setzer, A., Vermote, E., Reagan, J. A., Kaufman, Y. J., Nakajima, T., Lavenu, F., Jankowiak, I., and Smirnov, A.: AERONET – a federated instrument network and data archive for aerosol characterization, Remote Sens. Environ., 66, 1–16, doi:10.1016/S0034-4257(98)00031-5, 1998.

Huebert, B. J., Bates, T., Russell, P. B., Shi, G., Kim, Y. J., Kawamura, K., Carmichael, G., and Nakajima, T.: An overview of ACE-Asia: strategies for quantifying the relationships between Asian aerosols and their climatic impacts, J. Geophys. Res., 108, 8633, doi:10.1029/2003JD003550, 2003.

IPCC: The Physical Science Basis, Contribution of Working Group I to the Fifth Assessment Report of the Intergovernmental Panel on Climate Change, edited by: Stocker, T. F., Qin, D., Plattner, G.-K., Tignor, M., Allen, S. K., Boschung, J., Nauels, A., Xia, Y., Bex, V., and Midgley, P. M., Cambridge University Press, Cambridge, UK and New York, NY, USA, 2013.

ACPD
14, 27881–27944, 2014

Kaiser, J. F. and Reed, W. A.: Data smoothing using low-pass digital filters, Rev. Sci. Instrum., 48, 1447–1457, doi:10.1063/1.1134918, 1977.
King, M. D., Kaufman, Y. J., Menzel, W. P., and Tanré, D.: Remote sensing of cloud, aerosol, and water vapor properties from the moderate resolution imaging spectrometer (MODIS), IEEE T. Geosci. Remote, 30, 2–27, doi:10.1109/36.124212, 1992.
Klett, J. D.: Lidar inversion with variable backscatter/extinction ratios, Appl. Optics, 24, 1638–1643, doi:10.1364/AO.25.000833, 1985.
Law, K. S., Stohl, A., Quinn, P. K., Brock, C., Burkhart, J., Paris, J.-D., Ancellet, G., Singh, H. B., Roiger, A., Schlager, H., Dibb, J., Jacob, D. J., Arnold, S. R., Pelon, J., and Thomas, J. L.: Arctic air pollution: new insights from POLARCAT-IPY, B. Am. Meteorol. Soc., doi:10.1175/BAMS-D-13-00017.1, in press, 2014.
Lebel, T., Parker, D. J., Flamant, C., Bourlès, B., Marticorena, B., Mougin, E., Peugeot, C., Diedhiou, A., Haywood, J. M., Ngamini, J. B., Polcher, J., Redelsperger, J.-L., and Thorncroft, C. D.: The AMMA field campaigns: multiscale and multidisciplinary observations in the West African region, Q. J. Roy. Meteor. Soc., 136, 8–33, doi:10.1002/qj.486, 2010.
Matthias, V., Freudenthaler, V., Amodeo, A., Balin, I., Balis, D., Bösenberg, J., Chaikovsky, A., Chourdakis, G., Comeron, A., Delaval, A., de Tomasi, F., Eixmann, R., Hågård, A., Komguem, L., Kreipl, S., Matthey, R., Rizi, V., Rodrigues, J. A., Wandinger, U., and Wang, X.: Aerosol lidar intercomparison in the framework of the EARLINET project, 1. Instruments, Appl. Optics, 43, 961–976, doi:10.1364/AO.43.000961, 2004.
Mattis, I., Ansmann, A., Müller, D., Wandinger, U., and Althausen, D.: Dual-wavelength Raman lidar observations of the extinction-to-backscatter ratio of Saharan dust, Geophys. Res. Lett., 29, 1306, doi:10.1029/2002GL014721, 2002.
Measures, R. M.: Laser Remote Sensing: Fundamentals and Applications, Wiley, New York, 1984.
Molina, L. T., Madronich, S., Gaffney, J. S., Apel, E., de Foy, B., Fast, J., Ferrare, R., Herndon, S., Jimenez, J. L., Lamb, B., Osornio-Vargas, A. R., Russell, P., Schauer, J. J., Stevens, P. S., Volkamer, R., and Zavala, M.: An overview of the MILAGRO 2006 Campaign: Mexico City emissions and their transport and transformation, Atmos. Chem. Phys., 10, 8697–8760, doi:10.5194/acp-10-8697-2010, 2010.
Müller, D., Mattis, I., Wandinger, U., Ansmann, A., Althausen, D., and Stohl, A.: Raman lidar observations of aged Siberian and Canadian forest fire smoke in the free troposphere over

ACPD
14, 27881–27944, 2014

Germany in 2003: microphysical particle characterization, J. Geophys. Res., 110, 17201, doi:10.1029/2004JD005756, 2005.
Müller, D., Ansmann, A., Mattis, I., Tesche, M., Wandinger, U., Althausen, D., and Pisani, G.: Aerosol-type-dependent lidar ratios observed with Raman lidar, J. Geophys. Res., 112, 16202, doi:10.1029/2006JD008292, 2007.
Murayama, T., Müller, D., Wada, K., Shimizu, A., Sekiguchi, M., and Tsukamoto, T.: Characterization of Asian dust and Siberian smoke with multi-wavelength Raman lidar over Tokyo, Japan in spring 2003, Geophys. Res. Lett., 31, 23103, doi:10.1029/2004GL021105, 2004.
Nicolae, D., Nemuc, A., Müller, D., Talianu, C., Vasilescu, J., Belegante, L., and Kolgotin, A.: Characterization of fresh and aged biomass burning events using multiwavelength Raman lidar and mass spectrometry, J. Geophys. Res., 118, 2956–2965, doi:10.1002/jgrd.50324, 2013.
Panchenko, M. V., Zhuravleva, T. B., Terpugova, S. A., Polkin, V. V., and Kozlov, V. S.: An empirical model of optical and radiative characteristics of the tropospheric aerosol over West Siberia in summer, Atmos. Meas. Tech., 5, 1513–1527, doi:10.5194/amt-5-1513-2012, 2012.
Pappalardo, G., Amodeo, A., Pandolfi, M., Wandinger, U., Ansmann, A., Bösenberg, J., Matthias, V., Amiridis, V., De Tomasi, F., Frioud, M., Larlori, M., Komguem, L., Papayannis, A., Rocadenbosch, F., and Wang, X.: Aerosol lidar intercomparison in the framework of the EARLINET project, 3. Raman lidar algorithm for aerosol extinction, backscatter, and lidar ratio, Appl. Optics, 43, 5370–5385, doi:10.1364/AO.43.005370, 2004.
Paris, J.-D., Ciais, P., Nédélec, P., Stohl, A., Belan, B. D., Arshinov, M. Y., Carouge, C., Golitsyn, G. S., and Granberg, I. G.: New insights on the chemical composition of the Siberian Air Shed from the YAK-AEROSIB Aircraft Campaigns, B. Am. Meteorol. Soc., 91, 625–641, doi:10.1175/2009BAMS2663.1, 2010.
Raes, F., Bates, T., McGovern, F., and Van Liedekerke, M.: The 2nd Aerosol Characterization Experiment (ACE2): general overview and main results, Tellus B, 52, 111, doi:10.1034/j.1600-0889.2000.00124.x, 2000.
Raut, J.-C. and Chazette, P.: Retrieval of aerosol complex refractive index from a synergy between lidar, sunphotometer and in situ measurements during LISAIR experiment, Atmos. Chem. Phys., 7, 2797–2815, doi:10.5194/acp-7-2797-2007, 2007.
Royer, P., Raut, J.-C., Ajello, G., Berthier, S., and Chazette, P.: Synergy between CALIOP and MODIS instruments for aerosol monitoring: application to the Po Valley, Atmos. Meas. Tech., 3, 893–907, doi:10.5194/amt-3-893-2010, 2010.

ACPD
14, 27881–27944, 2014

Royer, P., Chazette, P., Lardier, M., and Sauvage, L.: Aerosol content survey by mini N2-Raman lidar: application to local and long-range transport aerosols, Atmos. Environ., 45, 7487–7495, doi:10.1016/j.atmosenv.2010.11.001, 2011.
Salomonson, V. V, Magner, T., Barnes, W., Montgomery, H., and Ostrow, H.: Moderate Resolution Imaging Spectrometer – a progress report (April 1989), in: Quantitative Remote Sensing: An Economic Tool for the Nineties, Proceedings of IGARSS '89 and of the 12th Canadian Symposium on Remote Sensing, Vancouver, Canada, Volume 5, IEEE, New York, 2917–2921, 1989.
Savitzky, A. and Golay, M. J. E.: Smoothing and differentiation of data by simplified least squares procedures, Anal. Chem., 36, 1627–1639, doi:10.1021/ac60214a047, 1964.
Ter Haar Romeny, B. M., Florack, L. M. J., Salden, A. H., and Viergever, M. A.: Higher order differential structure of images, in: Information Processing in Medical Imaging, edited by: Barrett, H. H. and Gmitro, A. F., Springer, Berlin, Heidelberg, 77–93, 1993.
Tesche, M., Gross, S., Ansmann, A., Müller, D., Althausen, D., Freudenthaler, V., and Esselborn, M.: Profiling of Saharan dust and biomass-burning smoke with multiwavelength polarization Raman lidar at Cape Verde, Tellus B, 63, 649–676, doi:10.1111/j.1600-0889.2011.00548.x, 2011.
Tikhonov, A. E. and Arsenin, V. Y.: Solutions of Ill-posed Problems, Wiley, New York, 1977.
Vautard, R., Menut, L., Beekmann, M., Chazette, P., Flamant, P. H., Gombert, D., Guédalia, D., Kley, D., Lefebvre, M.-P., Martin, D., Mégie, G., Perros, P., and Toupance, G.: A synthesis of the Air Pollution Over the Paris Region (ESQUIF) field campaign, J. Geophys. Res., 108, 8558, doi:10.1029/2003JD003380, 2003.
Welton, E. J., Campbell, J. R., Spinhirne, J. D., and Scott, V. S.: Global monitoring of clouds and aerosols using a network of micro-pulse lidar systems, in: Lidar Remote Sensing for Industry and Environmental Monitoring, Proc. SPIE 4153, edited by: Singh, U. N., Itabe, T., and Sugimoto, N., Sendai, Japan, 151–158, doi:10.1117/12.417040, 2001.
Whiteman, D.: Application of statistical methods to the determination of slope in lidar data, Appl. Optics, 38, 3360–3369, doi:10.1364/AO.38.003360, 1999.
Winker, D. M., Pelon, J. R., and McCormick, M. P.: The CALIPSO mission: spaceborne lidar for observation of aerosols and clouds, in: Lidar Remote Sensing for Industry and Environment Monitoring III, Proc. SPIE 4893, edited by: Singh, U. N., Itabe, T., and Liu, Z., Hangzhou, China, 1–11, doi:10.1117/12.466539, 2003.

ACPD
14, 27881–27944, 2014

Zhao, F., Tan, Y., Li, Z., and Gai, C.: The effect and correction of aerosol forward scattering on retrieval of aerosol optical depth from Sun photometer measurements, Geophys. Res. Lett., 39, L14805, doi:10.1029/2012GL052135, 2012.

ACPD
14, 27881–27944, 2014

Table 1. Values of the Backscatter to Extinction Ratio (BER) and Particle Depolarization Ratio (PDR) reported in the literature and observed in this study for desert dust aerosols, pure or mixed with biomass burning or pollution. For Burton et al. (2012), values are the 25–75th (5–95th) percentiles respectively. Bold numbers highlight observations made at the same wavelength as this study.

Aerosol type	Site, campaign	Instrument, inversion method	λ (nm)	BER (10^{-3} sr^{-1})	PDR (%)	Reference
Pure dust	AERONET network	Sun-photometer	550	24 ± 2	–	Cattrall et al. (2005)
	North America, multi campaign	High spectral resolution lidar	532	20–23 (18–24)	31–33 (30–35)	Burton et al. (2012)
	Morrocco and Cape Verde, SAMUM	N_2 Raman lidar	**355**	19 ± 3	26 ± 6	Tesche et al. (2011)
	Maldives Islands, INODEX	N_2 Raman lidar	**355**	26 ± 4	–	Müller et al. (2007)
	Beijing (China)	N_2 Raman lidar	**355**	29 ± 4	–	Müller et al. (2007)
	Tokyo (Japan)	N_2 Raman lidar	**355**	20 ± 4	~ 20	Murayama et al. (2004)
	Niamey (Niger)	N_2 Raman lidar	**355**	26 ± 5	–	Chazette et al. (2007)
	Balearic islands, HyMeX	N_2 Raman lidar	**355**	16–21	16–19	Chazette et al. (2013)
Dusty mix	North America, multi campaign	High spectral resolution lidar	532	24–33 (16–67)	13–20 (10–28)	Burton et al. (2012)
	Mor./C. Verde, SAMUM	N_2 Raman lidar	**355**	15 ± 3	16 ± 4	Tesche et al. (2011)
	Niamey (Niger)	N_2 Raman lidar	**355**	15	–	Chazette et al. (2007)
Pure dust	Kazan, lower sub-layer	Full Raman inversion	**355**	13 ± 2	23 ± 2	This study
	Kazan, upper sub-layer	Multi-layer Raman constr.		22 ± 12	20 ± 2	
Dusty mix	Ishim	Multi-layer Raman constr.		11 ± 5	15 ± 2	
Pure dust	Omsk	Full Raman inversion		23 ± 4	21 ± 4	

ACPD
14, 27881–27944, 2014

Table 2. Same as Table 1 but for biomass burning aerosols, either freshly emitted or aged. When the Backscatter to Extinction Ratio (BER) and the Particle Depolarization Ratio (PDR) have been retrieved at different wavelengths, the two values of wavelength are given.

Aerosol type	Site, campaign	Instrument, inversion method	λ (nm)	BER 10^{-3} sr^{-1}	PDR (%)	Reference
Fresh smoke	North America, multi campaign	High spectral resolution lidar	532	22–29 (19–42)	3–5 (2–8)	Burton et al. (2012)
	Bucharest, EARLINET	N_2 Raman lidar	**355**	14 ± 2	–	Nicolae et al. (2013)
Aged smoke	AERONET network	Sun-photometer	550	17 ± 2	–	Cattrall et al. (2005)
	North America, multi campaign	High spectral resolution lidar	532	14–18 (12–22)	4–9 (2–15)	Burton et al. (2012)
	Tokyo (Siberian smoke)	N_2 Raman lidar	**355**	~ 25	5–8	Murayama et al. (2004)
	Leipzig, EARLINET	N_2 Raman lidar	**355**–532	22 ± 6	< 5	Müller et al. (2005)
	Morrocco/Cape Verde, SAMUM	N_2 Raman lidar	**355**–532	11 ± 3	5 ± 2	Tesche et al. (2011)
	Bucharest, EARLINET	N_2 Raman lidar	**355**	20–31	–	Nicolae et al. (2013)
Aged smoke	Kazan	Partial Raman constraint	**355**	10 ± 2	1.9 ± 1.1	This study
	Ishim	Full Raman inversion		15 ± 1	3.2 ± 0.2	
	Omsk	Full Raman inversion		13 ± 2	3.5 ± 1.6	
	Niznheudinsk	Full Raman inversion		14 ± 2	0.9 ± 0.2	

ACPD
14, 27881–27944, 2014

Table 3. Same as Tables 1 and 2 but for pollution aerosols.

Site, campaign	Instrument, inversion method	λ (nm)	BER (10^{-3} sr^{-1})	PDR (%)	Reference
AERONET network	Sun-photometer	550	14 ± 2	–	Cattrall et al. (2005)
North America, multi campaign	High spectral resolution lidar	532	14–19 (13–24)	3–8 (2–11)	Burton et al. (2012)
Central Europe, EARLINET	N_2 Raman lidar	**355**–532	17 ± 4	< 5	Müller et al. (2007)
Paris, ESQUIF	Lidar/sun-phot. synergy	532	14–17	–	Chazette et al. (2005)
Paris, LISAIR	N_2 Raman lidar	**355**	11 ± 2	–	Raut and Chazette (2007)
Paris	N_2 Raman lidar	**355**	12 ± 2	–	Royer et al. (2011)
Po Valley	CALIOP/MODIS synergy	532	14 ± 2	–	Royer et al. (2010)
Pearl River delta, China	N_2 Raman lidar	532	21 ± 3	–	Müller et al. (2007)
Beijing	N_2 Raman lidar	532	26 ± 5	–	Müller et al. (2007)
Omsk (residual layer)	Full Raman inversion	**355**	12 ± 4	3.5 ± 0.8	This study

ACPD
14, 27881–27944, 2014

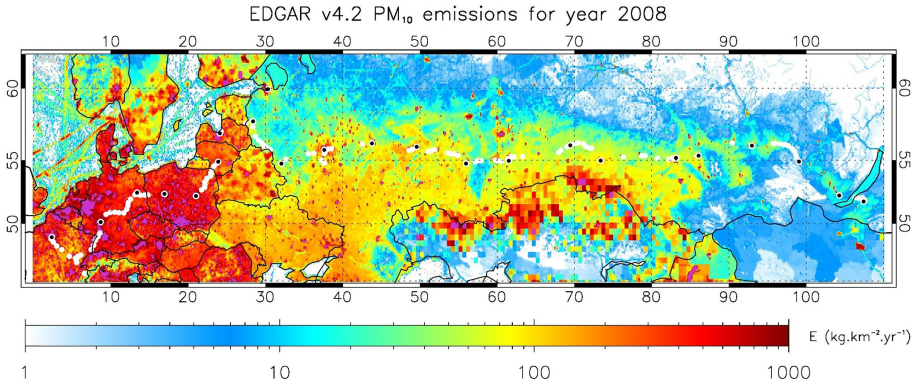

Figure 1. PM_{10} emissions for year 2008 from EDGAR v4.2 database (in kg km^{-2} year^{-1}). White and black dots show respectively the location of lidar measurements and of the main cities along the journey.

ACPD
14, 27881–27944, 2014

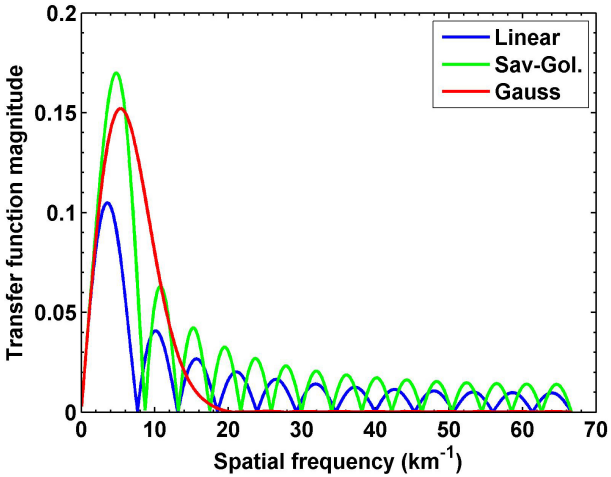

Figure 2. Magnitude of the transfer functions of three low-pass derivative filters: the linear least-square fit (blue), the Savitzky–Golay filter (green) and the Gaussian derivative filter (red). The Gaussian kernel was computed for a filter width $\sigma = 4$, then the kernel size of the two other filter was adjusted to produce the same cut-off frequency ($\sim 11\,\mathrm{km}^{-1}$), defined as $1/e$ of the magnitude maximum amplitude.

ACPD
14, 27881–27944, 2014

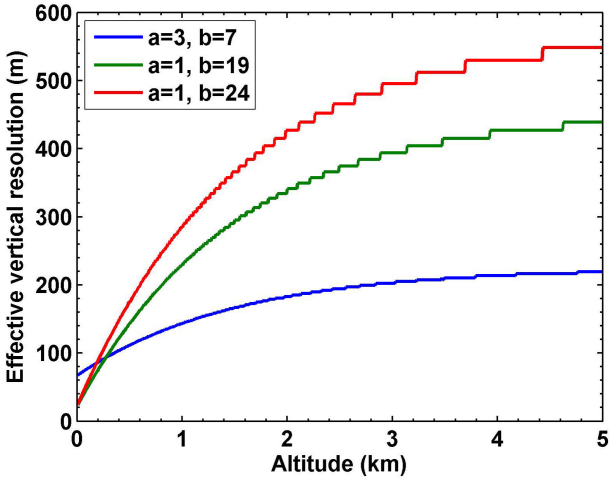

Figure 3. Effective vertical resolution of the extinction profile retrieved from the Raman optical depth using the Gaussian low-pass derivative filter, plotted for several sets of parameters. To answer the decrease of the signal to noise ratio with the distance from the lidar, the filter width is increased following $\sigma(z) = a + b \cdot \left(1 - \exp(-z/1.5)\right)$ where z is the altitude above ground level (in km). The effective vertical resolution is the inverse of the spatial cut-off frequency of the filter (see Fig. 2).

ACPD
14, 27881–27944, 2014

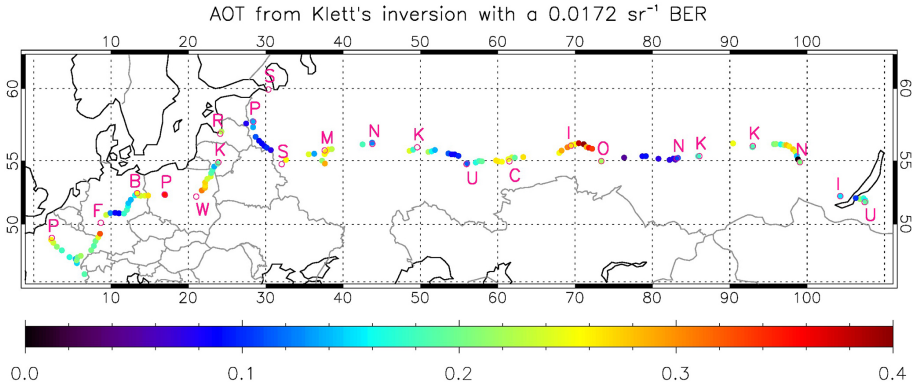

Figure 4. Map of the 355 nm Aerosol Optical Thickness (AOT) computed from the 30 min average profiles inverted using Klett's inversion with the campaign average Backscatter to Extinction Ratio (BER = 0.017 sr^{-1}). Pink circles show the main cities, from West to East: Paris, Frankfurt, Berlin, Poznań, Warsaw, Kaunas, Riga, Pskov, Saint-Petersburg (not in the transect), Smolensk, Moscow, Nizhniy-Novgorod, Kazan, Ufa, Chelyabinsk, Ishim, Omsk, Novosibirsk, Kemerovo, Krasnoyarsk, Nizhneudinsk, Irkutsk and Ulan-Ude.

ACPD
14, 27881–27944, 2014

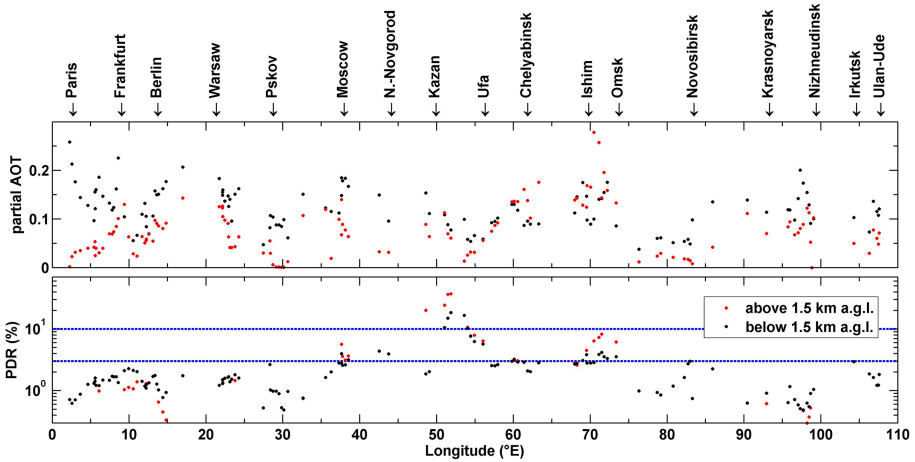

Figure 5. Partial Aerosol Optical Thickness (AOT, top) and average Particle Depolarization Ratio (PDR, bottom) along the route, computed below (in black) and above (in red) 1500 m a.g.l. All values are computed from the 30 min average profiles inverted using Klett's inversion and the campaign average Backscatter to Extinction Ratio (BER = 0.017 sr^{-1}). The average PDR is computed only when the scattering ratio is greater than 1.005. The blue dashed lines indicate the boundaries between pollution or biomass burning aerosols (below 3 % PDR), a mixing of different types, and desert dust aerosols (above 10 %).

ACPD
14, 27881–27944, 2014

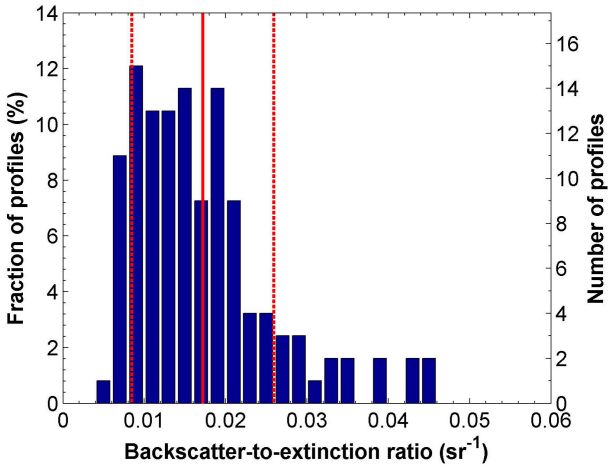

Figure 6. Distribution of the Backscatter to Extinction Ratio (BER) values obtained from the 30 min average profiles by constraining Klett's inversion with the partial aerosol optical thickness provided by the Raman channel between 0.3 and 0.7 km a.g.l. Profiles from Istomino village (Lake Baikal shore) have been removed and only the 124 profiles for which the agreement was better than 10^{-3} were included in the histogram. The red lines represent the BER average value and 1-σ SD.

ACPD
14, 27881–27944, 2014

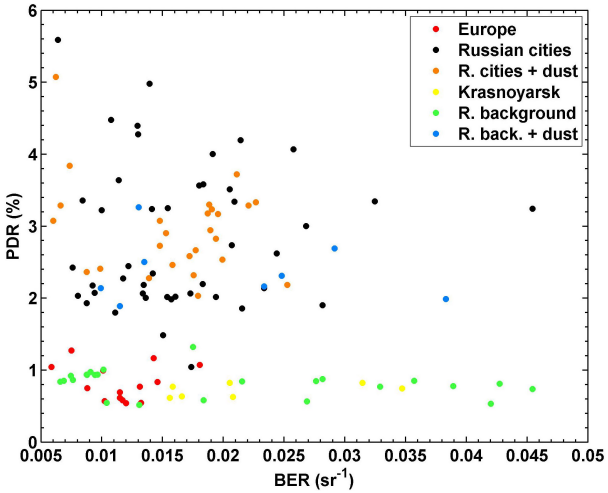

Figure 7. Average Particle Depolarization Ratio (PDR) in the constraint zone (0.3–0.7 km a.g.l.) vs. Backscatter to Extinction Ratio (BER) values for the 124 convergent 30 min profiles for 6 types of atmospheric and geographic conditions (apart from Istomino village). Here, PDR was computed using the campaign average BER (0.017 sr^{-1}).

ACPD
14, 27881–27944, 2014

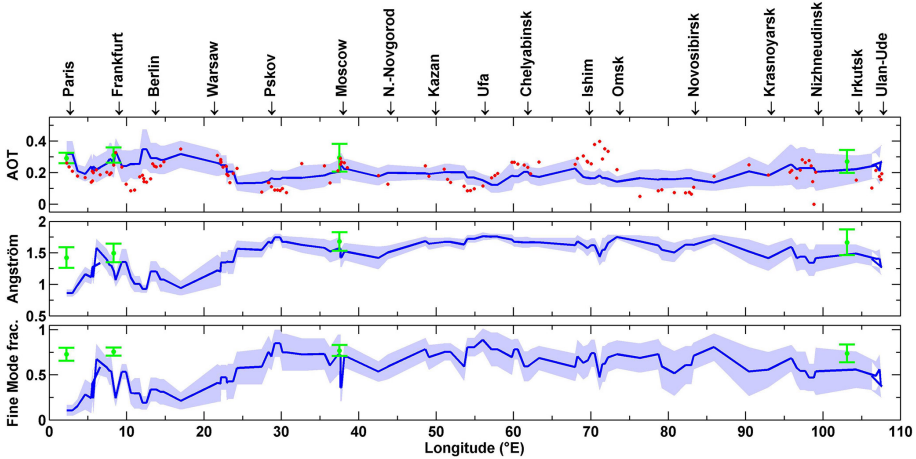

Figure 8. (top) Aerosol Optical Thickness (AOT) at 355 nm from the lidar (red), from MODIS Terra (blue) and from the AERONET stations along the transect (green). (middle) Ångström coefficients from MODIS Terra (470–660 nm) and from AERONET (440–675 nm). (bottom) AOT small mode fraction from MODIS Terra (550 nm) and from AERONET (500 nm). For MODIS (MOD08_M3 product), the $1^\circ \times 1^\circ$ pixels including the van position were extracted and the months of June from years 2000 to 2013 (except years 2001, 2003 and 2012 due to intense fire events) were used to compute MODIS average and SD (blue line and shading). For AERONET, only data since 2006 were used since only Palaiseau (2.5° E) has data prior to this year.

ACPD
14, 27881–27944, 2014

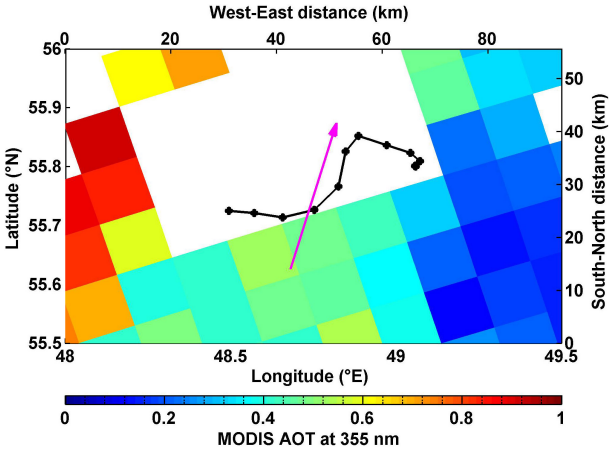

Figure 9. Location of the 5 min average lidar profiles (black dots) recorded on 18 June 2013 West of Kazan (the city is at the right end of the trajectory) and MODIS Aerosol Optical Thickness (AOT) at 355 nm from the Terra overpass at 09:20 UTC on the same day. The pink arrow represents the wind direction in the dust layer from ECMWF ERA-Interim reanalysis (12:00 UTC and 750 hPa pressure level).

ACPD
14, 27881–27944, 2014

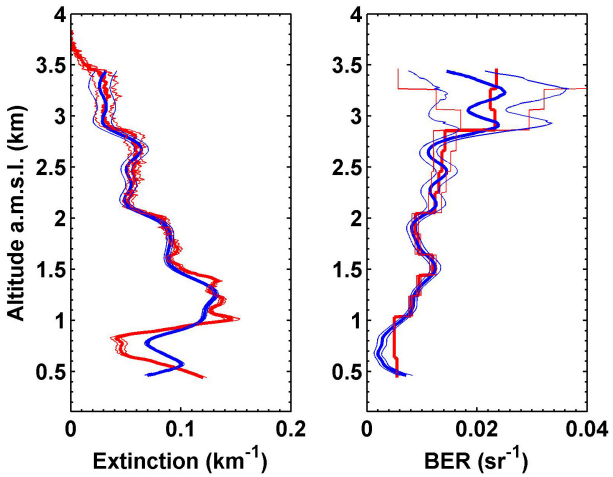

Figure 10. Vertical profiles of aerosol extinction and Backscatter to Extinction Ratio (BER) determined from the 55 min average profile on 18 June 2013, using either the low-pass derivative filter inversion (blue) or the constrained Klett procedure on a sliding 200 m window (red). Thick and thin lines are the average and 1-σ SD from the Monte-Carlo process. For these mobile observations, the altitude is above mean sea level (a.m.s.l.); the ground average altitude was around 0.1 km a.m.s.l.

ACPD
14, 27881–27944, 2014

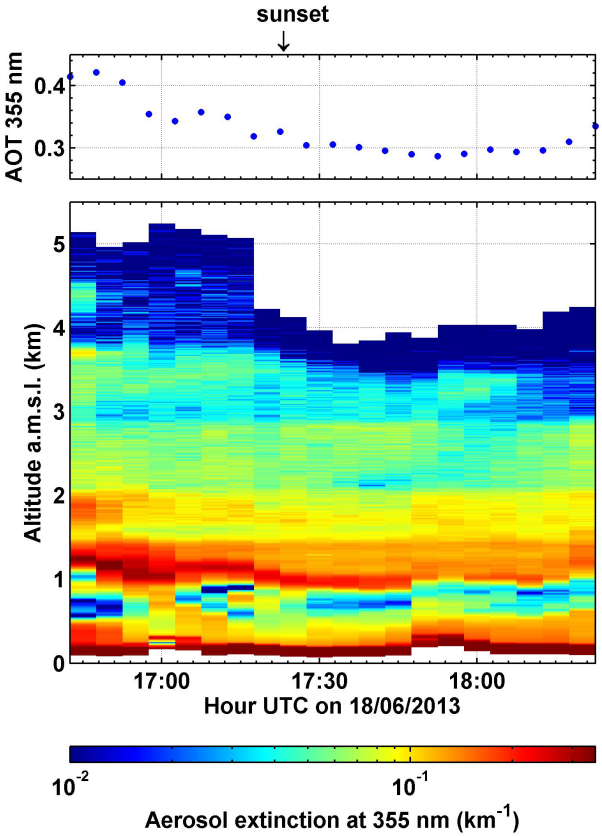

Figure 11. Aerosol extinction and optical thickness (AOT) observed West of Kazan on 18 June 2013 twilight as a function of UTC time and altitude above mean sea level (a.m.s.l.). Retrieval was made using a Klett inversion with the backscatter to extinction ratio profile from the sliding-window constrained Klett procedure (Fig. 10).

ACPD
14, 27881–27944, 2014

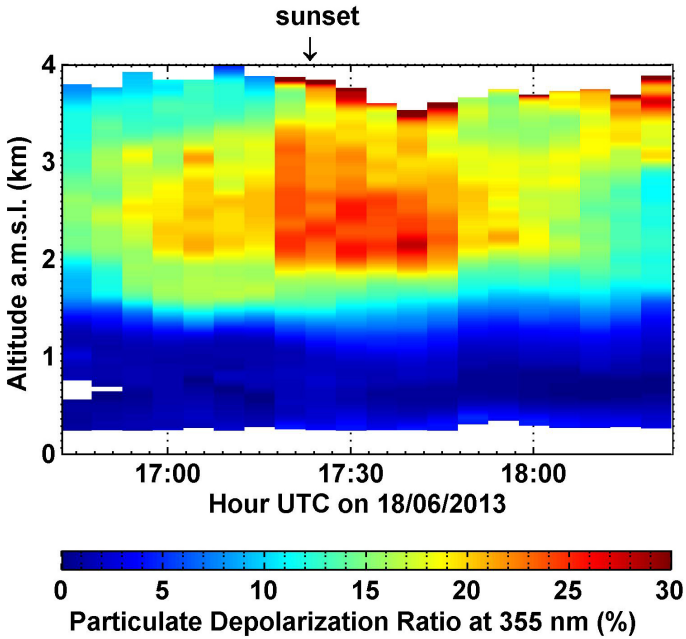

Figure 12. Particle Depolarization Ratio (PDR) observed West of Kazan on 18 June 2013 twilight as a function of UTC time and altitude above mean sea level (a.m.s.l.).

ACPD
14, 27881–27944, 2014

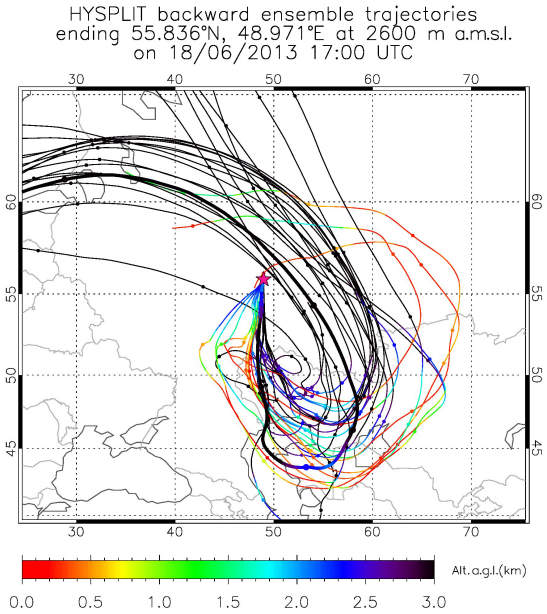

Figure 13. Seven-day back-trajectories ending in the dust layer observed west of Kazan city on 18 June 2013, computed using HYSPLIT Lagrangian model in single (bold line) and ensemble mode (thin lines). Trajectories are colored following the altitude above ground level (a.g.l.): red parts correspond to ground contact. Ticks are spaced by 24 h.

ACPD
14, 27881–27944, 2014

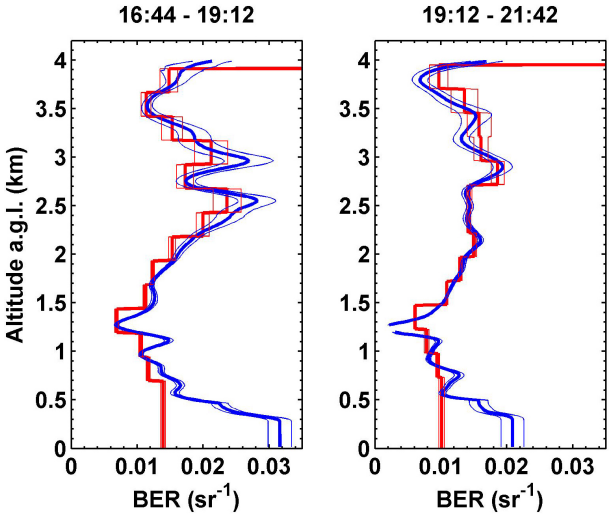

Figure 14. Profiles of Backscatter to Extinction Ratio (BER) retrieved above Omsk city on 23 June 2013 from two different processes: (red) profiles from the sliding-window constrained Klett process, (blue) profiles from the low-pass derivative filter inversion.

ACPD
14, 27881–27944, 2014

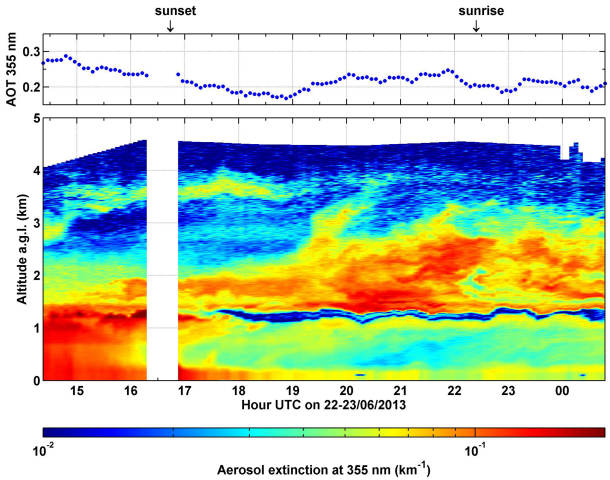

Figure 15. Aerosol Optical Thickness (AOT, up) and extinction (bottom) retrieved above Omsk during the night from 22–23 June 2013 as a function of UTC time and altitude above ground level (a.g.l.). Retrieval was made using a Klett inversion with the backscatter to extinction Ratio profiles from Fig. 14.

ACPD
14, 27881–27944, 2014

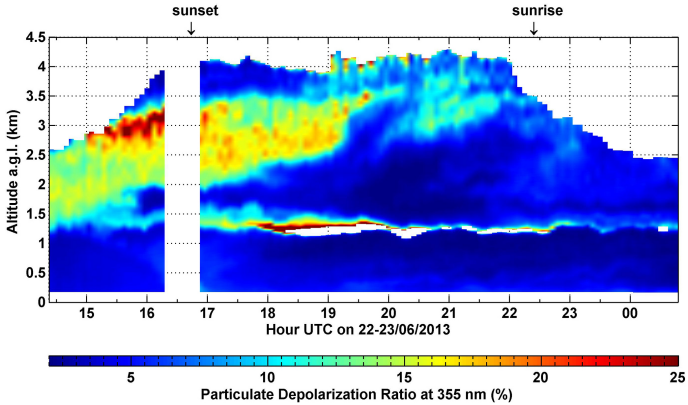

Figure 16. Particle depolarization ratio retrieved above Omsk during the night of 22–23 June 2013 as a function of UTC time and altitude above ground level (a.g.l.).

ACPD
14, 27881–27944, 2014

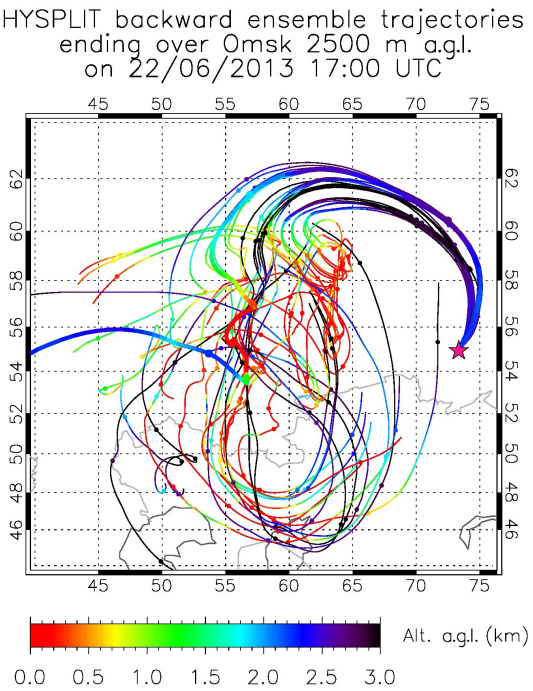

Figure 17. Seven-day back-trajectories ending in the dust layer observed above Omsk city on 22 June 2013, computed using HYSPLIT Lagrangian model in single (bold line) and ensemble mode (thin lines). Trajectories are colored following the altitude above ground level (a.g.l.): red parts correspond to ground contact. Ticks are spaced by 24 h.

ACPD
14, 27881–27944, 2014